Advanced Numerical and Experimental Transient Modelling of Water and Gas Pipeline Flows Incorporating Distributed and Local Effects

YOUNG IL KIM

Thesis for Doctor of Philosophy (PhD)
School of Civil, Environmental and Mining Engineering
July 2008

CHAPTER 8

THE EFFECT OF ORIFICE AND BLOCKAGE ON TRANSIENT PIPE FLOWS

The unique dynamic behaviour of pressure waves affected by flow system components and pipeline abnormalities causes a major obstacle in the development of a precise transient analysis model for a pipeline. Understanding the interaction among different system components is important for system design and calibration. This research investigates the dynamic characteristics of orifices and blockages (axial-extended orifices) that may affect the shape and phase of transient pressure waves due to energy dissipation and dispersion. The dynamic flow behaviour through a pipe restriction can be represented by three different energy loss factors, which include the irreversible energy loss (net or permanent pressure loss) by turbulent jet flow, the kinetic pressure difference represented by the instantaneous flow acceleration and deceleration, and pressure wave dispersion by eddy inertia of the jet flow. The study proposes instantaneous inertia and frequency-dependent models to describe the kinetic pressure difference. The traditional steady-state characteristics of an orifice are used to calculate the net pressure loss, and the wave dispersion by turbulent jet flow is considered by the wavespeed adjustment method. This research presents a number of case studies of how these abnormalities affect pressure wave in a pipeline system by laboratory tests. An experimental investigation has been carried out for the tank-pipeline-valve system with various orifices and blockages.

8.1 INTRODUCTION

Unsteady flow in pipeline systems offers a challenge of flow analysis, particularly when there is interaction between different system facilities. Changes of pipe diameter and material, valves, orifices, leakages, blockages, joints, junctions, complex boundary conditions, and other non-pipe elements commonly encountered in pipeline systems provide unique unsteady behavioural characteristics during periods of rapid pressure or flow changes. These unsteady characteristics create a major obstacle in the development of a precise transient analysis model or its practical applications because of the lack of knowledge of the dynamic behaviour of various components in the pipeline systems. Pipeline assessment and fault detection systems based on a transient model require the detailed knowledge of pressure wave attenuation and variation of pressure wave shape. The difficulties are in the high order effects involving energy dissipation and dispersion, high dimensional reflections, and non-linear behaviour during rapid transients. The development of an appropriate and accurate numerical dynamic model for transients is an essential prerequisite for pipeline design and system calibration.

An orifice is a widely employed device for measuring or regulating the flow of fluids owing to its simplicity and low cost. Also, orifices are important elements from the viewpoint of pipeline system design because they can adequately represent many flow system components, such as valves, blockages, leakage, and joints. An orifice plate measures the rate of fluid discharge based on empirically steady-state characteristics obtained from the great volume of research data [ASME, 1959; BSI, 1964; Doebelin, 1990; Fietz, 1988; Goldstein, 1983; Murdock, 1976; Spitzer, 1991]. An orifice plate acts as a constriction in a pipe that produces a region of increased velocity and reduction in pressure across the plate as shown in Fig. 8.1. The difference in pressure Δp between upstream and downstream pressure tappings, such as flange, radius, vena contracta, and pipe taps, may be related to the volumetric flow rate Q.

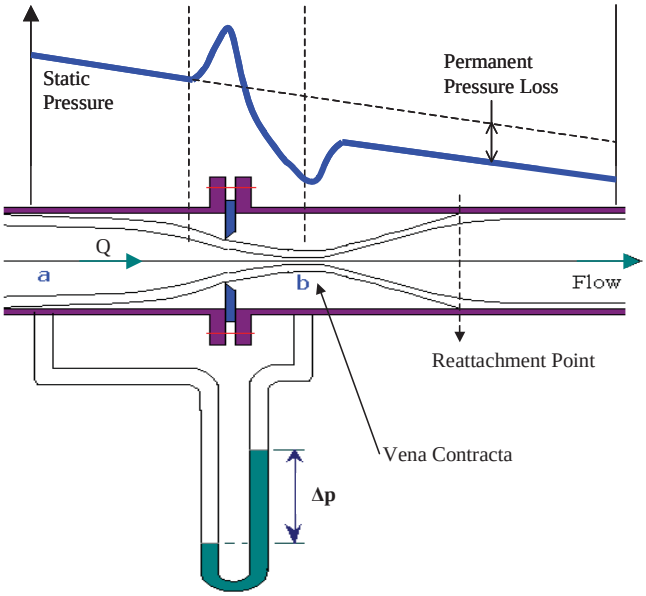

Figure 8.1 Orifice Plate showing Variation of Pressure along the Pipe

After a fluid passes through the orifice bore restriction, the flow velocity increases very rapidly and the pressure drops abruptly. This is the conversion of potential energy to kinetic energy. As a fluid flows through an orifice, the bore restriction of an orifice generates a convergent jet flow that continues to contract for a short distance downstream of the orifice plate before it diverges to fill the pipe at the reattachment point. The minimum cross-section of the jet flow is known as the *vena contracta* with minimum pressure and maximum velocity. When the fluid leaves the *vena contracta*, its velocity decreases and its pressure increases as kinetic energy is converted back into potential energy. Although the flow velocity at the downstream of the orifice recovers to the velocity of the upstream, the pressure does not reach quite the value that it would have had in the absence of the device. There is a permanent pressure loss (net pressure loss; irreversible pressure change) across the restriction due to the energy dissipation by turbulent eddies of the jet flow.

Flow restrictions can be subjected to cavitation if the velocity is high or the pressure low. Cavitation is one of the considerable problems in the pipeline systems because of its offensive noise, resulting vibrations, possible erosion damage, and its effect on the discharge coefficient. Tullis [1989] demonstrated the generation of turbulent eddies and cavitation process by pipeline restrictions, such as valves, orifices, elbows, and tees that create large pressure drops. When the jet flow through the restrictions enters the

downstream enlargement, an intense shear layer is created along the boundary between the jet and the surrounding separation region. The high velocity in the shear layer generates eddies. The pressure inside eddies is significantly less because of its high rotational speed. If nuclei are entrained in the eddies and the pressure drops to vapour pressure, the gas cavities will begin to grow by vapourization. Tullis [1989] and Tullis and Govindaraja [1973] indicated that cavitation is so difficult to predict because the time-dependent pressures generated by turbulence or the formation and decay of eddies are an important part of the cavitation process. The pressure inside separation regions, eddies, and vortices can only be estimated from empirical data.

The flow characteristics of water passing through very small sharp-edged cylindrical orifices and small opening valves with different shapes have been investigated by numerical and experimental approaches [Bikai et al., 2002; Ramamurthi and Nandakumar, 1999; Wu et al., 2003]. They determined the flow characteristics in the orifice by the separated, attached, and cavitated flow regions. The experimental data of Bikai et al. [2002] and Ramamurthi and Nandakumar [1999] indicated that, with all orifice diameters, with an increase in the aspect ratio (axial length of orifice / orifice bore diameter) there is a decrease in the possibility of cavitation and at the same aspect ratio, the possibility of cavitation is lower when the diameter of the orifice is large. This means that cavitation occurs more easily when the orifice diameter is small and the axial length of orifice is short. Also, when cavitation occurs, the flow coefficients (see Eq. 8.1) are always lower than those of non-cavitating flow owing to the occurrence of cavitation and the existence of two-phase friction loss.

A methodology for designing various orifice-meters has been developed by many researchers. The quadratic equation of Eq. 8.1 is commonly used to model the flow through hydraulic orifices. Borutzky et al. [2002] proposed the orifice flow model for laminar and turbulent flow conditions. They indicated that the derivative of the flow with respect to the pressure drop tends to infinity when the pressure drop approaches zero in the quadratic relationship. Moreover, it is more reasonable to assume that the flow depends linearly on the pressure drop for very small values of the pressure drop. Zhang and Chai [2001] studied hydraulic characteristics of multistage orifice tunnels to dissipate a large amount of energy at the design discharge and water level in the large-scale hydraulic projects. They investigated orifice geometry to meet energy dissipation requirements and

to minimize cavitation risk. In many industrial applications, the additional loss (permanent pressure loss and high system resistance) due to the flow meter is not desirable and the need for an alternate type of metering device arose. Sondh et al. [2002] and Singh et al. [2004] examined the design and development of variable area orifice meter with a bluff body to reduce the additional loss by flow meter. Leakage from a pipeline is generally described by using orifice equation. Experimental and numerical investigations have been executed for examining the jet behaviour of pipeline leakage by considering the orifice shape and fluid pressure [Wakes et al., 2002; Oke et al., 2003; Al-Khomairi, 2005]. Many applications in the gas industry require the generation and measurement of gas flows. For this purpose, the ducts with constrictions may be used for measuring gas flow. Fujimoto and Usami [1984] and Jitschin [2004] investigated the gas flow through a circular orifice experimentally.

Blockages are common problems in the older pipeline systems. Echavez [1997] investigated the hydraulic behaviour of galvanized iron and copper pipes of ages between 15 and 50 years. They found that the diameter was reduced and the roughness increased with age in the galvanized iron pipes. For the copper pipes there was no appreciable change in these aspects with age. A blockage, which may be considered as an orifice with a significant axial-extended dimension, can be applied to orifice hydraulic component with additional inertia and resistance in the vicinity of the component.

Pipe flow can be severely curtailed by partial blockages, whose immediate impact is loss of deliverability and higher pumping costs [Adewumi et al., 2003]. They may also create water quality problems because stagnant fluid is left for extended periods of time. Blockages can arise from condensation, solid deposition, a pipeline dent (Cosham and Hopkins [2004]) by outside force, partially or fully closed valves due to operator error, discrete partial strictures, and extended pipe constrictions. Early detection of these blockages is necessary to monitor the economic impact of reduced flow rates and to prevent a total disruption of production due to complete blockage of the pipe. Fig. 8.2 shows examples of the blockages in pipelines.

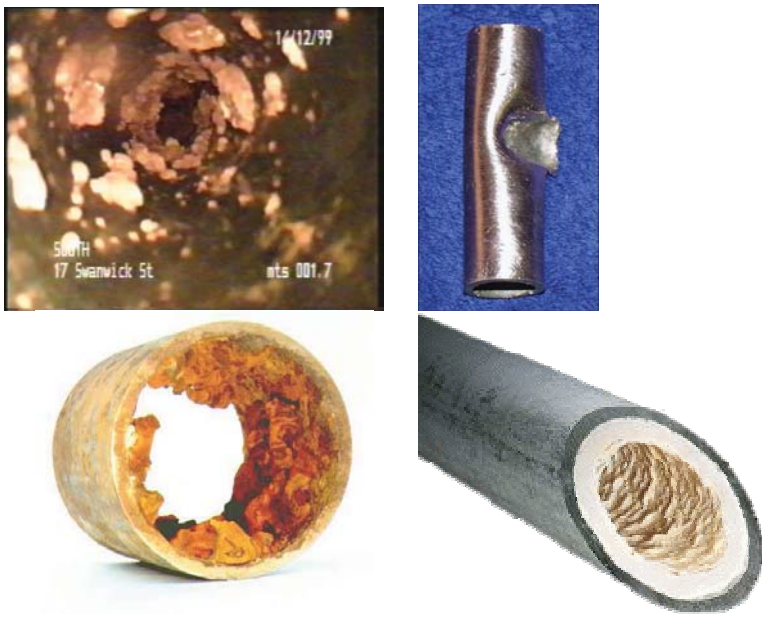

Figure 8.2 Blockages in a Pipeline System

Many studies of blockage detection and characterization have been reported. Qunli and Fricke [1989] presented the estimation of blockage dimensions in ducts based on the theoretical and experimental analyses of eigenfrequency shifts due to the presence of a blockage. De Salis and Oldham [2001], Stephens et al. [2003], Adewumi et al. [2003] examined the possibility of use the interaction between a pressure wave propagation by unsteady pipe flows with the pipeline blockages. Vítkovský et al. [2003] and Mohapatra et al. [2006] presented the methods for the detection and location of blockages by an impulse response method in the frequency domain. The pressure response was measured and the impulse response and transfer functions were determined for the system. An extra spike in the impulse response identified the presence of a blockage. Wang et al. [2005] developed blockage detection method using the blockage-induced transient damping based on the analytical solution expressed in terms of a Fourier series.

The unsteady characteristics of orifice and blockage flow are generally assumed to be identical with the steady-state characteristics. Although this approximation has been used extensively to describe the physical phenomena of flow system components during transients, the unsteady behaviour can deviate considerably from that predicted by steady characteristics [Moseley, 1966; Prenner, 1998]. Understanding the unsteady hydraulic resistance behaviour of the restriction of orifice and blockage is of great importance for the

dynamic calculations for pipeline design and assessment. Restrictions or blockages can cause excessive high-frequency pressure waves and dangerous pressure oscillations.

Surge tanks and hydropower systems usually use an orifice throttle to suppress the pressure waves caused by rapid changes of flow. The transmission and reflection of pressure wave generated by the surge tanks and hydropower systems with restrictions have been investigated to ensure waterhammer system control and to obtain more reliable system operation [Seth, 1973; Ramos and Almeida, 2001 and 2002; Van Duyne et al., 2003]. The prediction of the pressure difference and flow rate due to the pulsation flow is an interesting subject for both an academic and practical viewpoint. Experimental and numerical approaches showed that if the pipe flow with incompressible or compressible fluids is of a pulsating nature, a large error in the flow measurement using orifice meters may result when the steady state characteristics are used [Earles and Zarek, 1963; Sparks, 1966; Moseley, 1966; De Bernardinis et al., 1981; Jones and Bajura, 1991]. The proposed pulsating flow techniques are inadequate to completely define the measurement error under pulsative flow conditions.

Many studies have been conducted for estimating the dynamic characteristics of unsteady flows through orifices. However, their results are unsatisfactory to consider the pressure wave transmission and reflection during transients with extended time period because the pipe restriction causes complex physical phenomena. Investigations have only focussed on the behaviour of pressure waves on the throttle element itself. Early research used the concept of the equivalent length (classical end correction as given by Rayleigh for acoustic inductance) to deal with linear and nonlinear acoustic impedance of circular orifices [Thurston and Martin, 1953; Thurston and Wood, 1953; Thurston et al., 1957]. However, this technique is just an approximation for predicting the flow characteristics of orifices. Daily et al. [1956] investigated the boundary resistance in unsteady motion for cases of form-type (pipeline restriction) resistance associated with the high shear and diffusion of turbulence accompanying jet formation. They found that the combined resistance of the orifice and the conduit was less than the equivalent steady-state cases during accelerating motion of flows and more than the equivalent steady-state cases during decelerated motion.

Contractor [1965] dealt with the reflection and transmission waves produced when a waterhammer pressure wave encountered an orifice. The comparison between measured

pressure data and his simulation results showed a significant discrepancy because the simulations that were executed based on classical wave theory with steady state characteristics and without considering unsteady resistance effects. Trengrouse et al. [1966] presented a comparison of unsteady flow discharge coefficients for sharp-edged orifices with steady flow values in the compressible pipe flow. The application of the steady flow values to unsteady flow conditions gave rise to significant errors. McCloy [1966] investigated the effects of fluid inertia and compressibility on the orifice flow meters operating under unsteady conditions.

Yamaguchi [1976] applied free streamline theory to the unsteady flow of incompressible fluid through an orifice. He considered two-dimensional irrotational motion of the flow. Ohmi et al. [1985b] investigated the velocity distribution and reattachment length in unsteady pipe flow through a plate orifce. Hayase et al. [1995] proposed a time-dependent calculation for a suddenly imposed pressure gradient through an orifice by using the concept of the equivalent length and two characteristic time constants that considered the timing of flow rate change and final settling of flow. Prenner [1998 and 2000] investigated the behaviour of in-line orifice in a straight pipe by using the first cycle of pressure surge. His experimental data indicated that the influence of additional inertia forces of the orifice flow, the delayed scaling-off of the boundary layer, cavitation and unsteady friction effects in the orifice flow are of significance when the ratio of areas (orifice / pipe cross-section area) is less than 1:64. Also, although he showed unsteady energy loss approach for an orifice by slightly modifying the unsteady friction model based on convolution weighting function, the unsteady coefficient for an orifice was determined by comparing with measured data.

8.2 NUMERICAL MODELS FOR PIPE RESTRICTIONS

The purpose of this research is to develop unsteady minor loss models that describe the dynamic behaviour of orifices and blockages (axial-extended orifices) during fast transients, which affect the magnitude, phase, and shape of unsteady pressure wave by energy dissipation and dispersion, higher dimensional pressure wave reflections, and nonlinear behaviour. When a pressure wave encounters any restriction such as an orifice, valve, or blockage, it produces a sudden energy loss. This research presents different two unsteady orifice flow models derived from instantaneous acceleration/deceleration flow

and its frequency dependent orifice flow to describe the kinetic pressure difference. The proposed model does not need to use measured data for finding unsteady coefficients for orifices and blockages under transient flow conditions. The unsteady coefficients are determined by analytical solutions. The traditional steady-state characteristics of a restriction are used to calculate the net pressure loss, and the wave dispersion by turbulent jet flow is considered by the wavespeed adjustment methods.

8.2.1 Steady-State Flow Models for Pipe Restrictions

The pressure change through an orifice is generally taken into consideration by the well-known relationship in Eq. 8.1 including discharge coefficient C_d that depends on the beta ratio (β = *orifice bore diameter d / pipe diameter D*), the location of the pressure tappings related to the plate and the Reynolds number.

$$Q = \frac{C_d A_o}{\sqrt{1-(A_o / A_p)^2}} \cdot \sqrt{\frac{2\Delta p}{\rho}} = E_f A_o \cdot \sqrt{\frac{2\Delta p}{\rho}} \tag{8.1}$$

where Q = flow rate, A_o = cross-section area of the restriction, A_p = pipe cross-section area, Δp = differential pressure through an orifice, and E_f = flow coefficient. The differential pressure for a given orifice meter increases almost in proportion to the square of flow rate. This steady-state equation of an orifice is used to calculate the net pressure loss by turbulent jet flow in this research.

For compressible fluid gas flow, the pressure loss across the restriction results in an expansion of the fluid at the restriction and the fluid density is not constant between the pipe and the restriction. The isentropic gas expansion factor Y is used to compensate for the expansion of the fluid at the restriction [Spitzer, 1991]. The mass flow rate equation for compressible fluid is

$$m = Y_{1\,or\,2} \cdot \frac{C_d A_o}{\sqrt{1-(A_o / A_p)^2}} \cdot \sqrt{2\rho_{1\,or\,2}\,\Delta p} = Y_{1\,or\,2} \cdot E_f A_o \cdot \sqrt{2\rho_{1\,or\,2}\,\Delta p} \tag{8.2}$$

The value of the expansion factor depends on the reference pressure. The subscript of gas expansion factor Y is 1 when the reference pressure is the upstream line pressure and the

subscript is 2 when the downstream pressure is the reference pressure. The gas expansion factor is given as

$$Y_1 = \frac{\sqrt{\left(1-\beta^4 \cdot \gamma/(\gamma-1) \cdot p_R^{2/\gamma}\right) \cdot \left(1-p_R^{(\gamma-1)/\gamma}\right)}}{\sqrt{\left(1-\beta^4 \cdot p_R^{2/\gamma}\right) \cdot \left(1-p_R\right)}}$$
$$Y_2 = Y_1 \frac{\sqrt{1}}{\sqrt{1-x_1}} = Y_1\sqrt{1+x_2} \qquad (8.3)$$

where p_R is the ratio of the absolute downstream line pressure to the absolute upstream line pressure, and γ is the specific heat ratio of the flowing fluid. x_1 is the ratio of the differential pressure to the absolute upstream line pressure, $(p_1-p_2)/p_1$ and x_2 is the ratio $(p_1-p_2)/p_2$ of the differential pressure to the absolute downstream reference pressure p_2.

This research uses the empirical equation (commonly referred to as API or AGA equation) defined by ANSI/API 2530, AGA Report-3, and GPA 8185-85 to predict the discharge coefficient of an orifice [Spitzer, 1991]. Eq. 8.1 or 8.2 with Eqs. 8.4a and 8.4b is used for calculating the net pressure loss across the orifice.

$$C_d = \sqrt{(1-\beta^4)} \cdot E_f \cdot [1 + d \cdot (905 - 5000\beta + 9000\beta^2 - 4200\beta^3 + 875/D)/N_{Rd}] \qquad (8.4a)$$

where

$$E_f = \frac{0.5925 + 0.0182/D + (0.440 - 0.06/D)\beta^2 + (0.935 + 0.225/D)\beta^5 + \\ +1.35\beta^{14} + (1.43/\sqrt{D}) \cdot (0.250-\beta)^{5/2}}{1.01358 - 0.075\beta + 0.135\beta^2 - 0.063\beta^3 + 0.0131/D} \qquad (8.4b)$$

where N_{Rd} is bore Reynolds number ($N_{Rd} = N_{RD}/\beta$). In the numerator of Eq. 8.4b for E_f, the last term becomes negative for some values of β. In such cases, this term is to be neglected and its value treated as zero. The net pressure loss across the orifice is updated by Eq. 8.1 to 8.4a at every time step during calculation of transient flows.

The shapes of blockages in real pipeline systems are arbitrary as shown in Fig. 8.2. It is very difficult to determine the exact shape of a blockage for numerical calculation and the actual shape of a natural blockage should be expressed in the 3-dimensional approach. However, highly dimensional approaches of unsteady flow analysis for water and gas

transmission or distribution pipeline systems would require tremendous computational time. In this research, the shape of a natural blockage is idealized as a significantly axial-extended orifice. Therefore, a blockage can be regarded as the combination of sudden contraction and expansion in a pipeline as shown in Fig. 8.3.

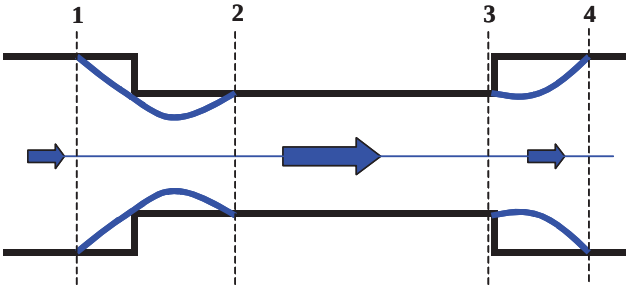

Figure 8.3 Blockage as the Combination of a Sudden Contraction and Expansion

The energy losses h_c and h_e due to sudden contraction and expansion in the pipe cross section can be calculated with both the energy and momentum equations for steady-state flows [Streeter and Wylie, 1985].

$$h_c = \left(\frac{1}{C_c} - 1\right)^2 \frac{V_2^2}{2g} \tag{8.5a}$$

$$h_e = \frac{(V_3 - V_4)^2}{2g} = \frac{V_3^2}{2g}\left(1 - \frac{A_3}{A_4}\right)^2 = \frac{V_3^2}{2g}\left[1 - \left(\frac{D_3}{D_4}\right)^2\right]^2 \tag{8.5b}$$

The contraction coefficient C_c for water of Eq. 8.5a is shown in Table 8.1.

Table 8.1 Contraction Coefficients

A_2/A_1	0.1	0.2	0.3	0.4	0.5	0.6	0.7	0.8	0.9	1.0
C_c	0.624	0.632	0.643	0.659	0.681	0.712	0.755	0.813	0.892	1.0

8.2.2 Unsteady Minor Loss Models

The details of the unsteady minor loss flow are still not completely understood because of the essential difficulty of its complex unsteadiness and high dimensional physical properties. Some two or three-dimensional models have been proposed to describe

unsteady characteristics across a restriction by including the actual velocity distribution, streamlines, and heat exchange in the research field of computational fluid dynamics. Although these models can provide more detail of the physical phenomena than one-dimensional approaches and present information needed to assess the validity of one-dimensional models, they just focus on the physical phenomena of the throttle element itself. Also, the practical application (extensive pipe network, real-time flow monitoring, pipeline fault detection and assessment using inverse analysis by evolution algorithm) of high-dimensional models is unreasonable when considering the requirement of significant large computational time and memory space.

The transmission and reflection of pressure waves at the pipe restriction are determined by the unsteady hydraulic resistance behaviour of the restriction. In this research, the unsteady energy loss across a restriction is considered to comprise of two kinds of energy loss phenomena in the transient pipe flow. One is a kinetic pressure difference caused by accelerating or decelerating fluid flows through the orifice. The other is the dispersion of pressure wave propagation by eddy inertia of a turbulent jet flow at the downstream side of the restriction. This research proposes two different models to evaluate the unsteady kinetic pressure difference. One is the instantaneous inertia model based on a time dependent description of the dynamic response of a restriction. The other is a frequency-dependent orifice flow model based on the rate of velocity changes at a restriction and the weighting function for the velocity changes. Finally, the wave dispersion by the eddy inertia of a turbulent jet flow is considered by the wavespeed adjustment methods.

1) Instantaneous Inertia Model

Funk et al. [1972] proposed a time dependent description of the dynamic response of orifices and very short lines (orifices with extended axial dimensions) based on accelerating and decelerating flows through a restriction. They also assumed that the irreversible pressure change (net pressure change) by turbulent jet flow across the orifice itself at any time could be described by steady-state energy considerations of Eq. 8.6.

$$p_u - p_d = \frac{\rho V^2}{2C_d^2} \tag{8.6}$$

where p_u and p_d are pressure upstream and downstream from an orifice. Eq. 8.6 is the same relationship that is normally used to describe steady-state orifice flow. This equation is obtained after neglecting the kinetic energy of the fluid approaching a restriction. The relationship for the dynamic characteristic of an orifice is expressed by a time dependent term representing the effect of accelerating and decelerating flow into and out of the orifice.

$$p_u - p_d = \rho A_o / \sqrt{\frac{C_d A_o \pi}{2}} \frac{dV}{dt} \tag{8.7}$$

For an orifice with significant axial dimension (blockage), both the inertia and the frictional resistance in the short section are added to the orifice equation. The flow in a circular tube can be assumed to act as transient plug flow that is considered as fully developed flow conditions because the radial dimension is short. The pressure drop in the circular tube is

$$\Delta p_t = \rho l_o \frac{dV}{dt} + \frac{\rho f l_o}{4 r_o} V^2 \tag{8.8}$$

where r_o is the radius of the orifice and l_o is the axial length of the blockage. In this research, the frictional resistance term is replaced with the unsteady friction model presented in Chapter 5. Finally, the pressure drop across the orifice or blockage is expressed by the sum of Eq. 8.6 to 8.8. This differential equation relates the flow through a restriction to the pressure drop across the restriction.

$$\Delta p = \left[\rho A_o / \sqrt{\frac{C_d A_o \pi}{2}} + \rho l_o \right] \frac{dV}{dt} + \left[\frac{\rho}{2 C_d{}^2} + \frac{\rho f l_o}{4 r_o} \right] V^2 \tag{8.9}$$

2) Frequency-Dependent Model

The transfer function (Eq. 8.10) for the kinetic pressure difference across an orifice and blockage was developed by using the wave equation for two-dimensional viscous flow in the frequency domain [Washio et al., 1996]. The transfer function is solved with the aid of

the Laplace transform, and the results of wave phenomena are given in the Laplace domain (s-plane).

$$\Delta p(s) = \rho\, j\omega A_o V(s)\left[2\psi_c\, G(r_o,\, r_p,\, j\omega) + \frac{l_o}{\pi r_o^2}\left\{\frac{I_0(z)}{I_2(z)}\right\}^2 \right]$$

where

$$G(r_o,\, r_p,\, s) \cong \frac{(1/r_o - 1/r_p)}{2\pi(1-\cos\varphi)} \cdot \left\{ \begin{array}{l} 1 + \cot\dfrac{\varphi}{2}\dfrac{(1/r_o + 1/r_p)}{2}\sqrt{\dfrac{\nu}{s}} \\ + \dfrac{(2+\cos\varphi)\cdot(1/r_o{}^2 + 1/r_o r_p + 1/r_p{}^2)}{6(1-\cos\varphi)}\dfrac{\nu}{s} \end{array} \right\} \tag{8.10}$$

where j = unit imaginary number, ω = angular frequency, ψ_c = correction factor for three different kinds of boundary conditions over the restriction (1.647 for uniform distribution of the normal velocities; 1.571 for uniform pressure; 1.724 for elliptic distribution of the normal velocities), r = pipe radius, $z = (a^2 s/\upsilon)^{0.5}$, I_0 and I_2 = modified Bessel functions of first kind of order 0 and 2, s = Laplace variable ($j\omega$), and φ = orifice conical angle with pipe axis. It is a necessary property of all Laplace transforms that they converge to zero when s tends through real values to + ∞. An examination of Eq. 8.10 leads to the result that $\Delta p(s)$ as a function of $V(s)$ does not satisfy this regularity. Therefore, $\Delta p(s)$ is expressed as a function of $\partial V(s)/\partial t$ by the definition of acceleration, $\partial V(s)/\partial t = sV(s)$, in the Laplace domain [Zielke, 1968].

$$\Delta p(s) = \rho\, A_o H(s) \frac{\partial V(s)}{\partial t}$$

$$\text{where } H(s) = 2\psi_c\, G(r_o,\, r_p,\, s) + \frac{l_o}{\pi r_o^2}\left\{\frac{I_0(z)}{I_2(z)}\right\}^2 \tag{8.11}$$

where $H(s)$ is the transfer function for unsteady kinetic pressure difference across a pipe restriction. This equation is the relation between the Laplace transformation of two-dimensional wave equation for the unsteady kinetic pressure difference across a pipe restriction and the acceleration. Frequency properties of pipeline systems can be calculated by putting $s = j\omega$ as shown in Eq. 8.11.

The properties of transient phenomena in the time domain (t-plane) are usually unobtainable due to the difficulties of the Laplace inversion. This research transforms the frequency properties (transfer function) of unsteady kinetic pressure difference across a restriction into the time domain (t-plane) to find time domain properties (impulse response) for unsteady kinetic pressure difference. The overall procedure of this transformation is expressed by linear time-invariant (LTI) system theory as shown in Fig. 8.4.

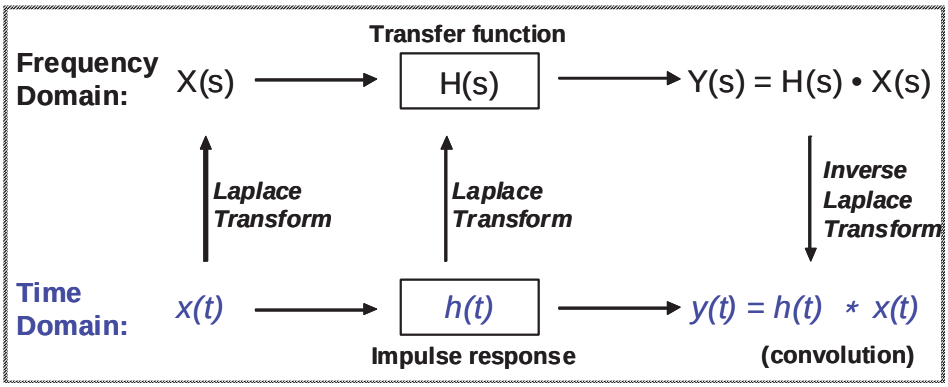

Figure 8.4 Linear Time-Invariant System

In the time domain point of view, the linear time-invariant systems can be characterized entirely by a single function called system's impulse response. The output of the system is the convolution of the input to the system and the system's impulse response. The convolution is a mathematical operator, which takes two functions, and produces a third function that in a sense represents the amount of overlap between two functions. Equivalently, LTI systems can be characterized in the frequency domain by the system's transfer function that is the Laplace transform of the system's impulse response. As a result of the properties of the Laplace transform, the output of the system in the frequency domain is the product of the transfer function and the Laplace transform of the input. The convolution in the time domain is equivalent to multiplication in the frequency domain.

Unfortunately, the transfer function for unsteady kinetic pressure difference across a restriction in Eq. 8.11 has no solution for direct transformation of inverse Laplace due to its complexity. Therefore, this research uses the numerical inversion of the Laplace transformation by approximating the transfer function. The values of transfer function are plotted in the s-plane, and are fitted by a least-squares nonlinear regression to find a fit

function that is the approximated transfer function $H'(s)$ and suitable for the direct inversion of Laplace transform. Eq. 8.12 shows the example of fitting function, which will be used to approximate the transfer function.

$$H'(s) = \frac{coeff\,1}{s + coeff\,2} + \frac{coeff\,3}{s + coeff\,4} + \ldots \tag{8.12}$$

The inversion of the approximated transfer function yields the impulse response for the unsteady kinetic pressure difference across a pipe restriction in the t-plane. The impulse response is expressed by the type of weighting function relating to past velocity changes. Fig. 8.5 shows the procedure of the numerical inversion of the Laplace transformation.

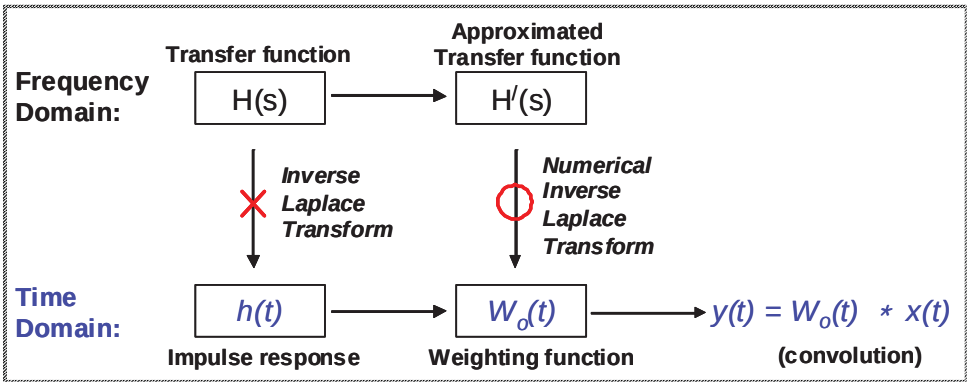

Figure 8.5 Numerical Inversion of Laplace Transformation

According to the linear time-invariant system theory, the output of a system (unsteady kinetic pressure difference) is represented by the convolution of the input (the rate of change of velocity) to the system and the system's impulse response (weighting function) in the time domain. The weighting function type equation in Eq. 8.13 gives the unsteady kinetic pressure difference through a pipe restriction. It is analogous with the unsteady pipe friction model presented in Chapter 5.

$$\Delta p(t) = \rho A_o \int_0^t \frac{\partial V}{\partial t}(\eta_t) W_o(t - \eta_t)\, d\eta_t \tag{8.13}$$

where η_t = reflection time of each event used in the convolution integral and W_o = weighting function for a restriction. This equation is added to the steady-state equation for calculating the net pressure loss and estimates the unsteady kinetic pressure difference for

pipeline restrictions during transients. Eq. 8.13 relates the unsteady kinetic pressure difference across a restriction in transient pipe flow to the instantaneous mean velocity and to the weighted past velocity changes, and is applied to the conservative solution scheme to calculate transient phenomena with pipeline restrictions.

In the time marching algorithm of the conservative solution scheme, the flow properties of the next step are calculated using the results of the previous time step. The history of the velocity is known. The unsteady kinetic pressure difference across a restriction can be calculated from a first-order approximation of Eq. 8.13 in the computational grid of the conservative scheme. The integral is approximated by using the trapezoid rule [Zielke, 1968].

$$\Delta p(t) = \rho A_o \int_0^t \frac{\partial V}{\partial t}(\eta_t) W_o(t-\eta_t) d\eta_t \cong \rho A_o \sum_{i=1,2,3...}^{n-1} (V^{n-i+1} - V^{n-i}) \cdot W_o(i\Delta t) \qquad (8.14)$$

where n = current computational time step. The weights of various orifices and blockages can be calculated from the above procedure requiring only the information of pipe diameter and restriction geometry. This procedure does not require the analysis of measured data to find the weighting functions (unsteady coefficient for a restriction). However, the weighting function is dependent on the selection of range of Laplace transform variable s (data range in the frequency domain) before executing the numerical inversion of Laplace transform, in which small values of s correspond to large values of real time t.

Zielke [1968] undertook the inverse Laplace transform analytically to obtain exact expression of the weighting function for unsteady wall friction in the transient laminar pipe flow. He decided on a range of Laplace variables based on small values (large times) and large values (small times) respectively. The inverse Laplace transform for the small Laplace variables was achieved by applying the residue theorem and the inverse transform for large variables was carried out by the approximations of a series for large values of s. Vardy and Brown [2003] used a simple function that approximated the transfer function for unsteady wall friction in the transient turbulent pipe flow. The simple function was valid for all variables and a simple inverse existed. The proposed approach in this research is similar to Vardy and Brown's method. However, unlike the wall shear stress, the pipe

restrictions, such as orifice, valve, or blockage, are discontinuous energy loss elements in the pipeline system. Therefore, it is difficult to find a fitting function for approximating the transfer function and proper Laplace variable range that satisfies all pipeline conditions. The fitting function and Laplace variable range should be calculated for each pipeline system with the geometry of pipe restrictions.

Figs. 8.6 and 8.7 show the examples of the calculated weights for the laboratory apparatus with various orifice bores when the orifice length (axial length) is 2 mm and with various axial-extended lengths (blockage) when the bore is 3 mm, and Table 8.2 and 8.3 are theirs weighting functions. The selected range of Laplace transform variables are from 0.1 to 1000 Hz. The greatest values of the weighting function occur at small times and the magnitudes of the weighting functions are much smaller at larger times. The values of the weighting function are bigger as the restriction bore is smaller and the axial dimension length is longer.

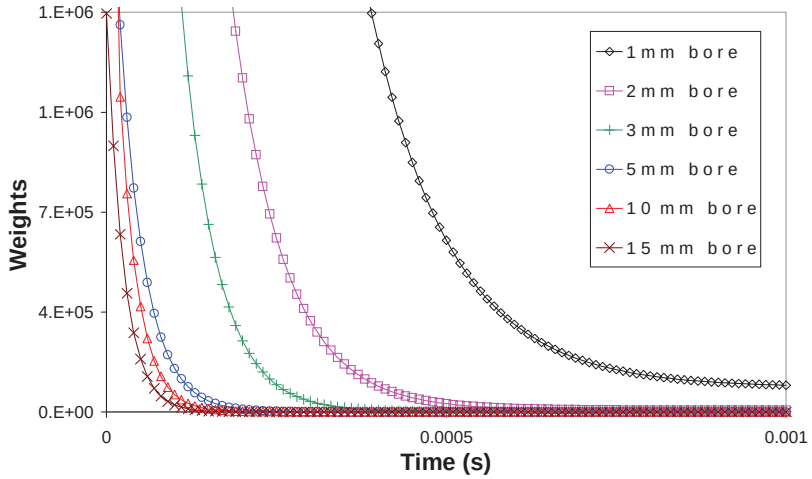

Figure 8.6 W_o for Various Orifice Bores

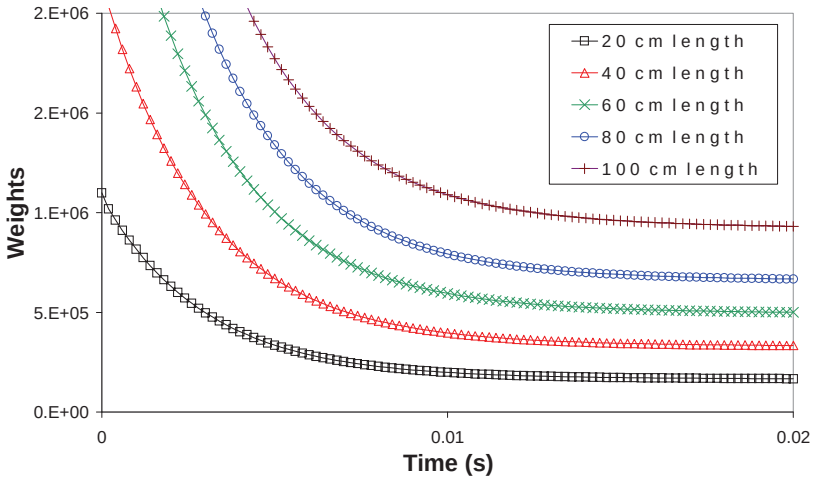

Figure 8.7 W_o for 3 mm Bore Blockage with Various Axial Lengths

Table 8.2 Weighting Functions for Various Orifice Bores

Weighting function	$coeff1e^{-coeff2 \cdot i\Delta t} + coeff3e^{-coeff4 \cdot i\Delta t}$			
Coefficients	**Coeff1**	**Coeff2**	**Coeff3**	**Coeff4**
0.5 mm Bore	1.3402e+8	8.5584e+3	1.3279e+6	5.8038e-4
1.0 mm Bore	8.6205e+4	3.2626e-3	3.5882e+7	8.4865e+3
2.0 mm Bore	6.2278e+3	0.015860	1.6169e+7	1.3156e+4
3.0 mm Bore	1.4936e+3	0.035480	1.2148e+7	1.9461e+4
5.0 mm Bore	2.1593e+6	1.5373e+4	2.1593e+6	1.5373e+4
10 mm Bore	1.1725e+6	2.7368e+4	1.1725e+6	2.7368e+4
15 mm Bore	6.9796e+5	4.0380e+4	6.9796e+5	4.0380e+4

Table 8.3 Weighting Functions for 3 mm Bore Blockage with Various Axial Lengths

Weighting function	$coeff1e^{-coeff2 \cdot i\Delta t} + coeff3e^{-coeff4 \cdot i\Delta t} + coeff5e^{-coeff6 \cdot i\Delta t} + coeff7e^{-coeff8 \cdot i\Delta t} + coeff9e^{-coeff10 \cdot i\Delta t}$				
Coefficients	**Coeff1**	**Coeff2**	**Coeff3**	**Coeff4**	**Coeff5**
20 cm length	9.0800e5	339.8055	1.7083e5	1.4004	8.3198e17
40 cm length	1.8279e18	9.5173e13	1.8143e6	340.0719	1.8283e18
60 cm length	4.2135e18	1.4662e14	4.2188e18	1.4663e14	4.2193e18
80 cm length	6.8211e5	1.3987	3.6271e6	340.2056	4.7609e18
100 cm length	5.3269e18	1.1123e14	5.3249e18	1.1129e14	4.5335e6

Table 8.3 (continued)

Weighting function	$coeff1e^{-coeff2 \cdot i\Delta t} + coeff3e^{-coeff4 \cdot i\Delta t} + coeff5e^{-coeff6 \cdot i\Delta t} + coeff7e^{-coeff8 \cdot i\Delta t} + coeff9e^{-coeff10 \cdot i\Delta t}$				
Coefficients	**Coeff6**	**Coeff7**	**Coeff8**	**Coeff9**	**Coeff10**
20 cm length	8.6165e13	8.3139e17	8.6144e13	8.3198e17	8.6150e13
40 cm length	9.5171e13	3.4126e5	1.3993	1.8279e18	9.5170e13
60 cm length	1.4662e14	2.7207e6	340.1610	5.1168e5	1.3989
80 cm length	1.2429e14	4.7636e18	1.2432e14	4.7616e18	1.2423e14
100 cm length	340.2324	5.3259e18	1.1125e14	8.5254e5	1.3985

8.3 EXPERIMENTAL VERIFICATION

Laboratory experiments have been carried out to verify the proposed unsteady minor loss models for orifice and blockage and to investigate the real physical phenomena of pipeline restrictions during transients. The experimental apparatus is described in detail in Chapter 4. The layout of the pipeline system is repeated in Fig. 8.8.

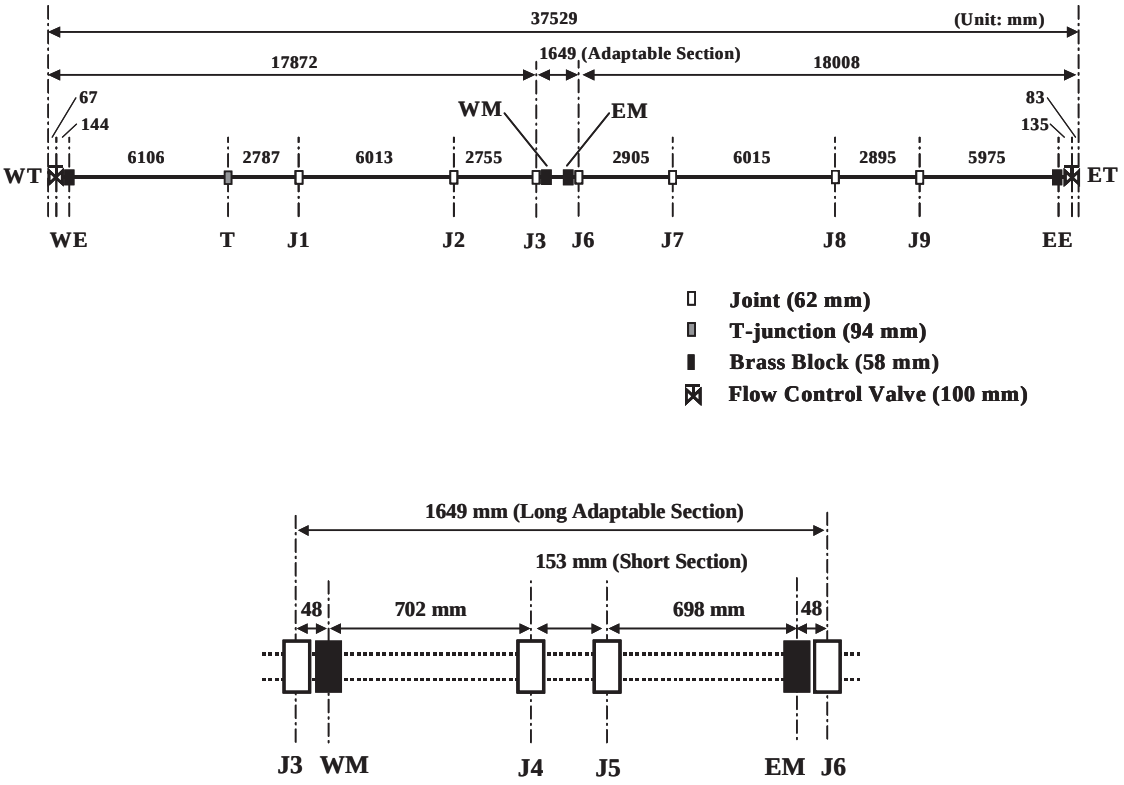

Figure 8.8 Pipeline System Layout

Transients are generated at WE by a side-discharge solenoid valve with fast operating time after closing the west flow control valve, thus the pipeline system can be regarded as tank-pipe-valve system. Pressures are monitored at 4 points (WE, WM, EM, EE) at brass blocks along the pipeline and at the bottom of both tanks. The sampling frequency of measured data is 4 kHz. Orifice tests have been executed by 2 mm thick brass orifice plates with 7 different square-edged concentric circular bores (0.5, 1, 2, 3, 5, 10, 15 mm), blockage tests have been conducted for both hard material blockages (brass and epoxy) and soft material blockages (silicon, Young's modulus E = 37.5 kPa) with 153 mm axial length and 5 different circular bores (2, 3, 5, 10, 15 mm). Orifices and blockages were located

between J4 and J5 as shown in Fig. 8.8. Figs. 8.9 and 8.10 show the installed orifice and blockage components in the middle of pipeline and Table 8.4 shows the beta ratio (β = *bore diameter d / pipe diameter D*) for orifices and blockages.

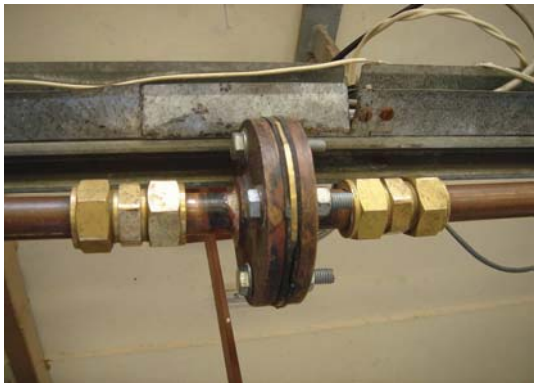

Figure 8.9 Orifice Components

Figure 8.10 Blockage Components

Table 8.4 Beta Ratios for Orifices and Blockages

Bore diameter for Orifice or Blockage	β
0.5 mm orifice	0.0226
1 mm orifice	0.0452
2 mm orifice or blockage	0.905
3 mm orifice or blockage	0.1357
5 mm orifice or blockage	0.2262
10 mm orifice or blockage	0.4525
15 mm orifice or blockage	0.6787

The initial steady-state velocities were estimated by the volumetric method. All transient tests for orifices and blockages were undertaken under the specified 6 different flow conditions (from laminar to low Reynolds number turbulent flow) by adjusting tank pressures. Table 8.5 shows the initial steady-state velocities.

Table 8.5 Initial Steady-State Velocities according to Test Conditions

Test Condition	Tank Pressure at ET (kPa)	Without a Restriction (m/s)	15 mm orifice (m/s)	10 mm orifice (m/s)	5 mm orifice (m/s)
Test Temperature		21°C	27°C	26°C	25°C
Condition 1	117.6	0.0599	0.0599	0.0599	0.0590
Condition 2	200.0	0.0824	0.0820	0.0821	0.0821
Condition 3	297.2	0.1031	0.1031	0.1031	0.1031
Condition 4	397.4	0.1208	0.1207	0.1208	0.1206
Condition 5	502.2	0.1368	0.1360	0.1367	0.1354
Condition 6	612.1	0.1495	0.1491	0.1490	0.1491

Table 8.5 Initial Steady-State Velocities according to Test Conditions (continued)

Test Condition	3 mm orifice (m/s)	2 mm orifice (m/s)		15 mm blockage (m/s)	10 mm blockage (m/s)	5 mm blockage (m/s)	3 mm blockage (m/s)
Test Temperature	25.5°C	27°C		19°C	20°C	19.5°C	19.5°C
Condition 1	0.0573	0.0498		0.0595	0.0598	0.0585	0.0550
Condition 2	0.0798	0.0699		0.0828	0.0831	0.0816	0.0776
Condition 3	0.0997	0.0848		0.1041	0.1040	0.1019	0.0957
Condition 4	0.1159	0.0993		0.1201	0.1203	0.1185	0.1117
Condition 5	0.1315	0.1128		0.1365	0.1346	0.1335	0.1258
Condition 6	0.1464	0.1239		0.1506	0.1497	0.1475	0.1397

8.3.1 Measured Transient Data of Pipeline with Orifices

Figs. 8.11 and 8.12 show the comparisons between the measured pressure data of intact (or unblocked) pipe (without an orifice and blockage) and the measured pressure data of pipeline with 5, 3, and 2 mm bore orifices under the various flow conditions shown in Table 8.5. The pressure data were measured at the end of pipeline (WE) and middle of pipeline (WM). The pressure data are plotted at the same scale graphs (pressure measure time: 1 second and measured pressure head range: 50 m) to compare each pressure variation, wavespeed, and pressure wave shape during same test condition. There is no transient pressure trace when the pipeline has 0.5 or 1 mm bore orifice because the orifices completely mitigate the pressure waves of transients. The initial pressure drops indicate the net pressure losses across the restrictions. As the bore size decreases, the magnitude of pressure wave dramatically decreases. The most important characteristics of measured

pressure data are the apparent changes in the wavespeed illustrated by the lagging and phase change of the pressure wave due to the reduction of bore size. The pressure data of 2 and 3 mm orifices show significant changes of pressure wavespeed.

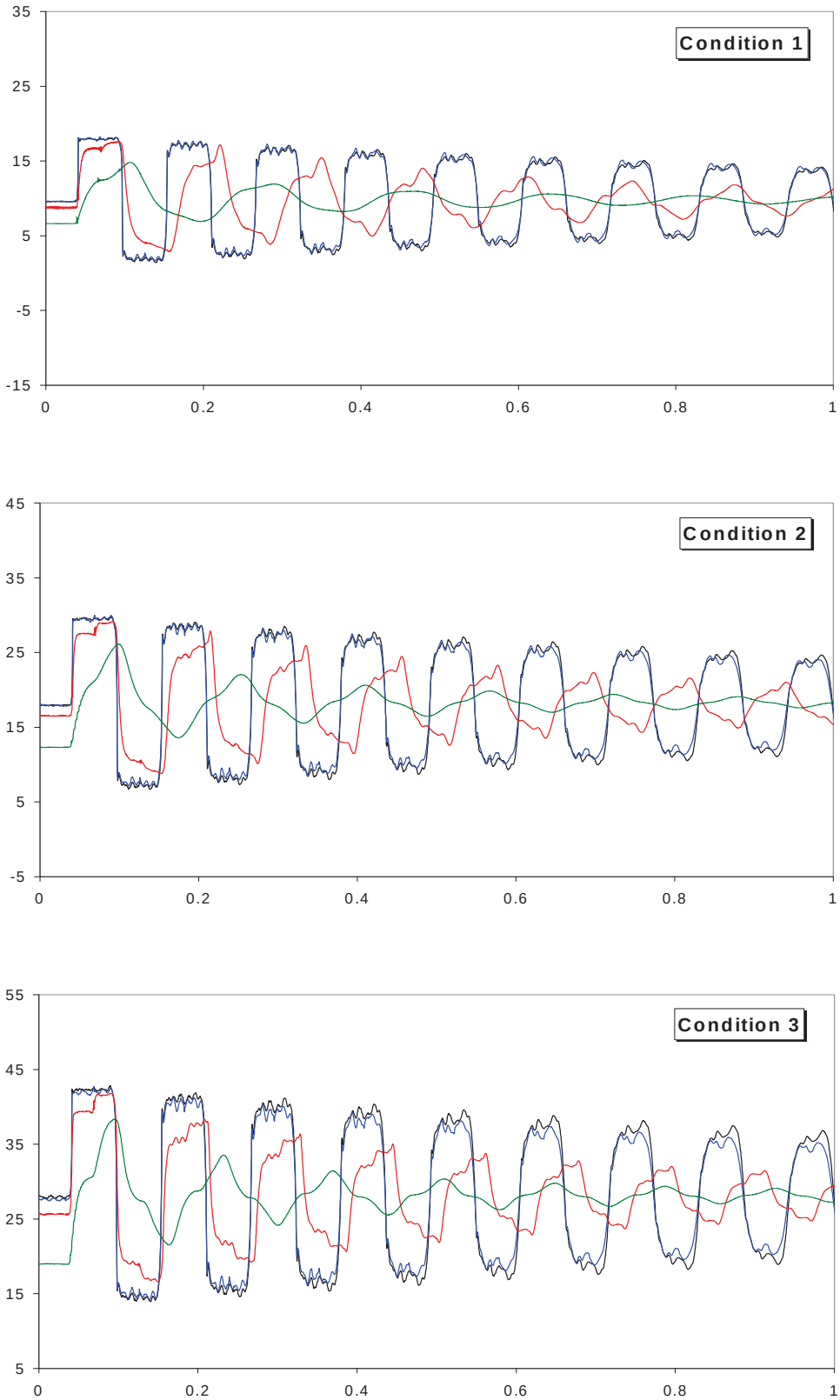

Figure 8.11 Measured Pressure Data (at WE) of Pipeline with Orifices

(The largest magnitude (black): intact or unblocked pipe, the second (blue): 5 mm orifice, the third (red): 3 mm orifice, the smallest magnitude (green): 2 mm orifice, x-axis: measurement time (s), and y-axis: pressure head (m))

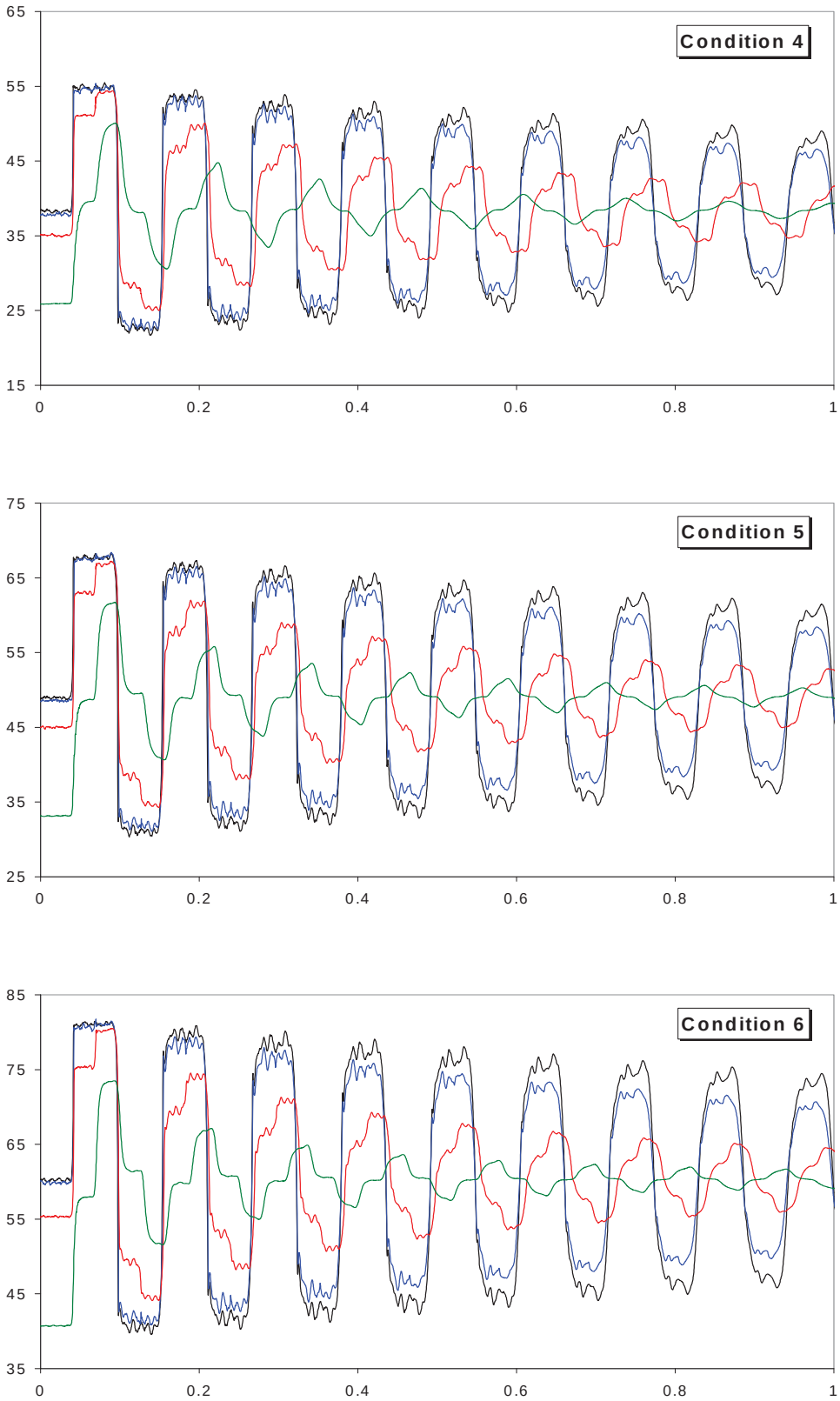

Figure 8.11 Measured Pressure Data (at WE) of Pipeline with Orifices (continued)

(The largest magnitude (black): intact or unblocked pipe, the second (blue): 5 mm orifice, the third (red): 3 mm orifice, the smallest magnitude (green): 2 mm orifice, x-axis: measurement time (s), and y-axis: pressure head (m))

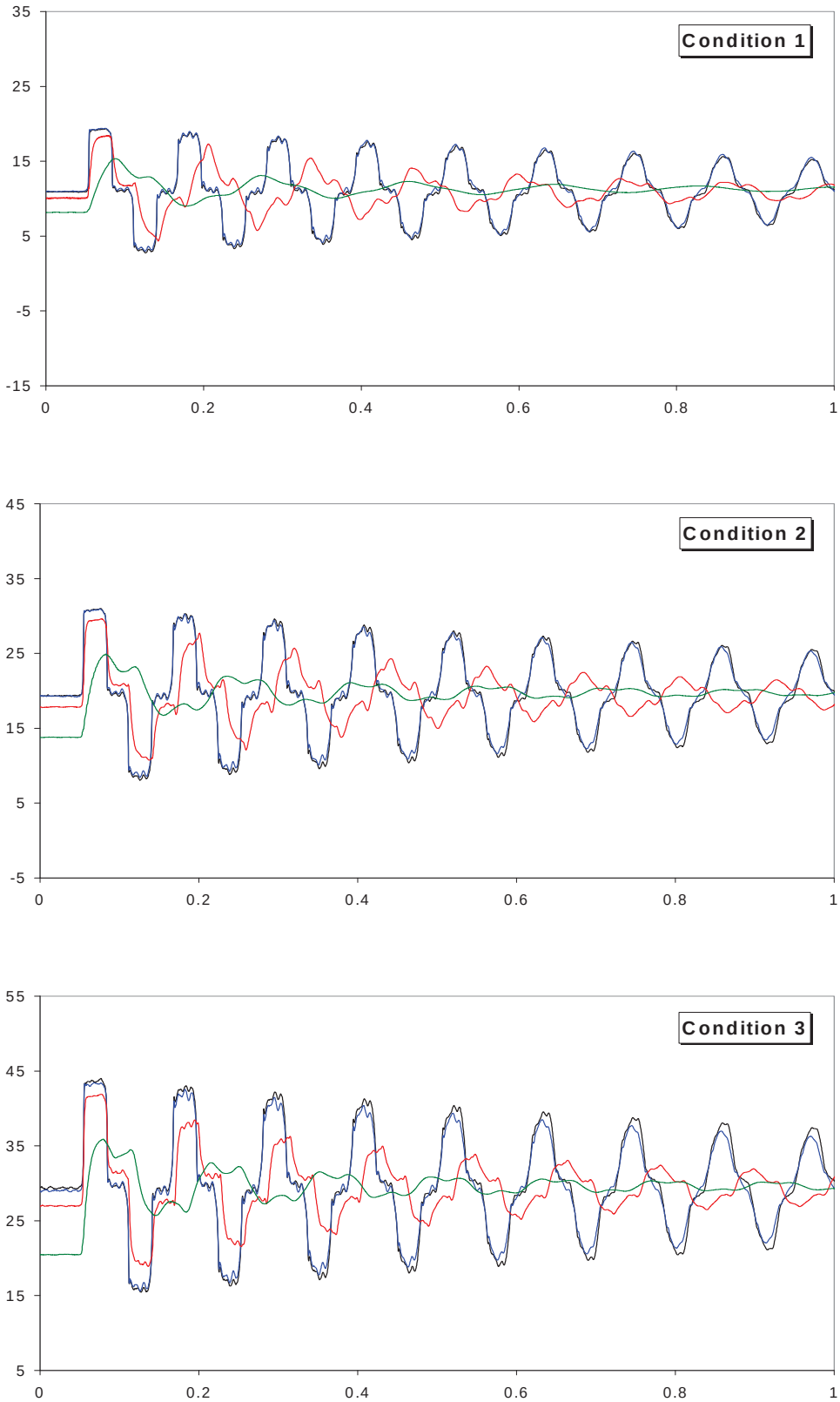

Figure 8.12 Measured Pressure Data (at WM) of Pipeline with Orifices

(The largest magnitude (black): intact or unblocked pipe, the second (blue): 5 mm orifice, the third (red): 3 mm orifice, the smallest magnitude (green): 2 mm orifice, x-axis: measurement time (s), and y-axis: pressure head (m))

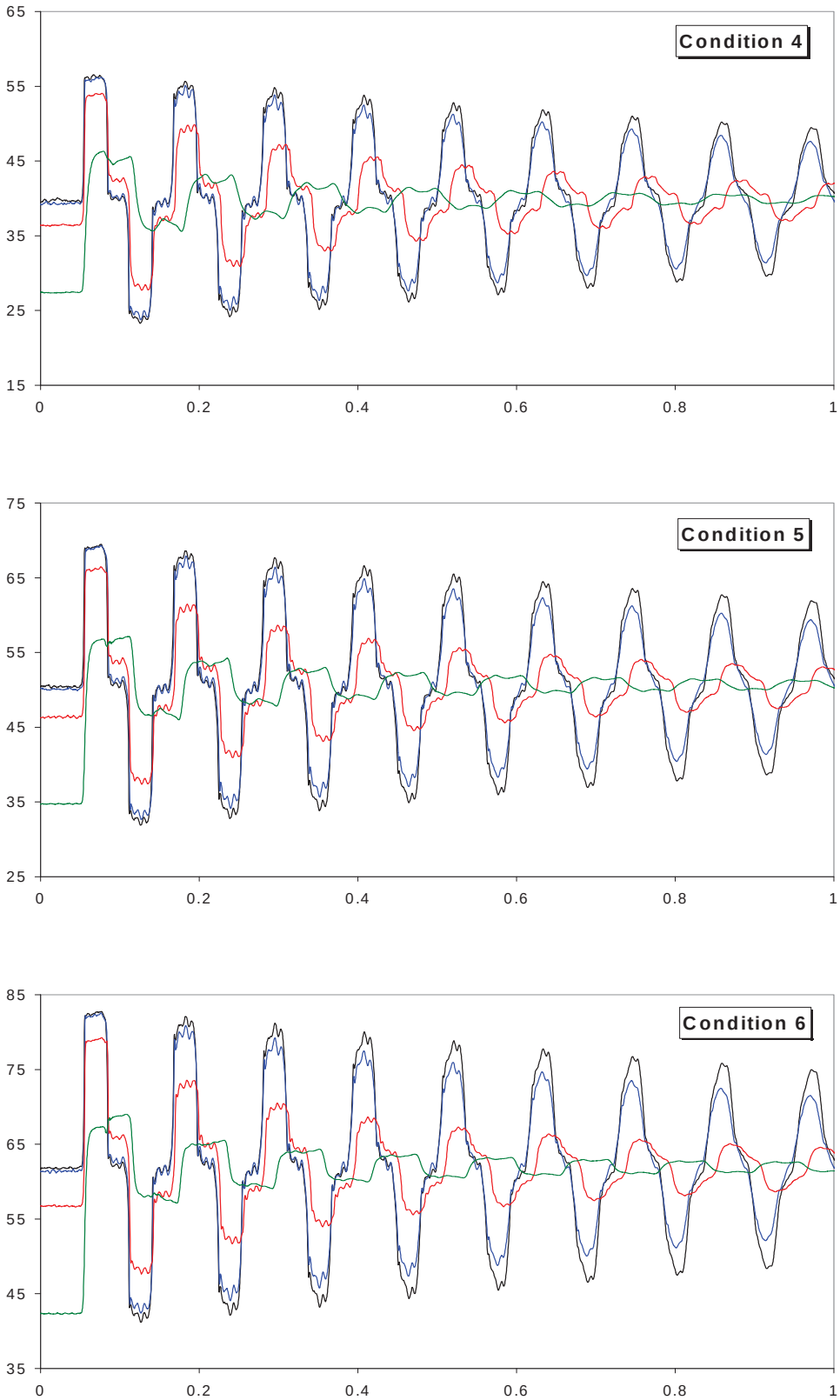

Figure 8.12 Measured Pressure Data (at WM) of Pipeline with Orifices (continued)

(The largest magnitude (black): intact or unblocked pipe, the second (blue): 5 mm orifice, the third (red): 3 mm orifice, the smallest magnitude (green): 2 mm orifice, x-axis: measurement time (s), and y-axis: pressure head (m))

Table 8.6 shows the initial pressure drop during steady-state flow condition due to 5, 3, and 2 mm orifices. The magnitude of pressure drop increases as the bore size of orifice decreases and the test pressure increases. Table 8.7 shows the wavespeeds of measured pressure waves by using the time between first and second pressure rise when the pipeline has a 2 or 3 mm orifice under various test conditions, although the wavespeeds are continually lagged as time goes on. The pressure propagation velocity is slower when the pipeline has a smaller restriction. It is difficult to find the exact reason for the wavespeed lagging effect. However, when the jet flow through the restrictions enters the sudden downstream enlargement, intense shear layer is created along the boundary between the jet and the surrounding separation region. The high velocity in the shear layer generates turbulent eddies. The pressure inside eddies is significantly less because of its high rotational speed. This low-pressure process by the high rotational speed may cause cavitations and gas release from a fluid. Therefore, the large pressure drop due to the turbulent eddies can reduce the velocity of pressure propagation. In an unsteady minor loss flow, eddies, which bear a role of nonlinear energy dissipation, repeat the cycle of development and reduction.

Table 8.6 Initial Pressure Drop by Orifices

	5 mm Orifice (m)	3 mm Orifice (m)	2 mm Orifice (m)
Condition 1	0.05	0.81	2.96
Condition 2	0.10	1.46	5.68
Condition 3	0.35	2.39	9.02
Condition 4	0.55	3.40	12.47
Condition 5	0.58	3.89	15.84
Condition 6	0.64	4.93	19.56

Table 8.7 Measured Wavespeeds for 2 and 3 mm Orifices

	Intact Pipe (m/s)	3 mm Orifice (m/s)	2 mm Orifice (m/s)
Condition 1	1334.4	1177.4	816.9
Condition 2	1331.4	1225.4	970.1
Condition 3	1334.4	1280.3	1097.7
Condition 4	1331.4	1302.5	1177.4
Condition 5	1331.4	1319.7	1205.7
Condition 6	1334.4	1319.7	1215.5

The detrained air can be easily collected at the pipeline restrictions as shown in the previous chapter. Fig. 8.13 shows the 3 mm orifice data affected by entrapped air at the orifice plate under the condition 1 (low pressure condition) and 5 (high pressure condition). The entrapped air causes the additional lag of wavespeed. The narrow spike of the first pressure rise indicates the existence of air pocket under the condition 1. The effect of air pocket on transients is less when the initial pressure condition is high because the initial size of air pocket is more contracted due to the larger pressure. The actual size of air pocket under the condition 5 is smaller than that in the condition 1. Under condition 5, the wavespeed almost recovers to the value without air pocket and the narrow spike of the first pressure rise vanishes.

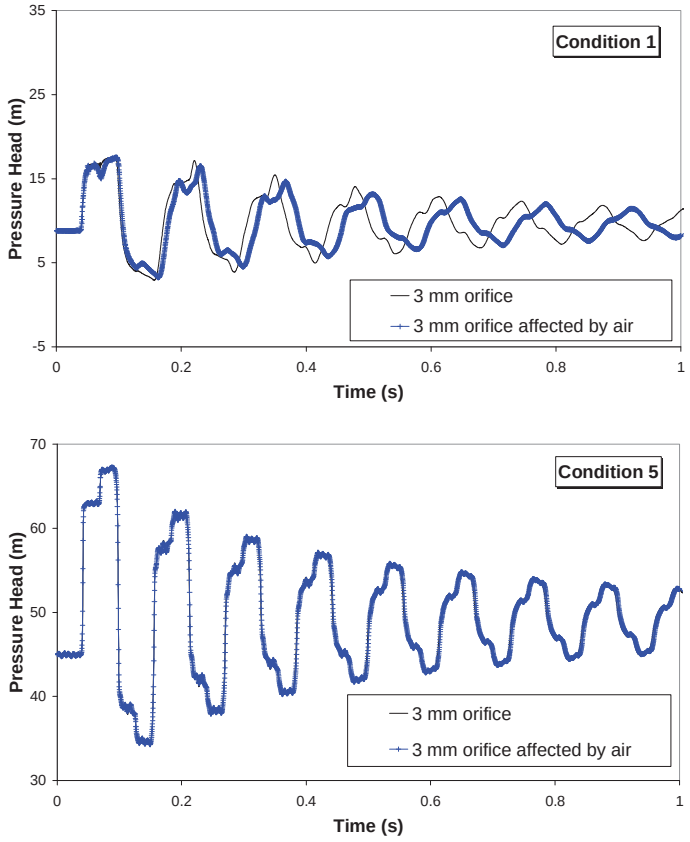

Figure 8.13 3 mm Orifice Data affected by Entrapped Air

Fig. 8.14 shows the comparisons between the measured pressure data of intact or unblocked pipe (without an orifice and blockage) and the measured pressure data of pipeline with 15 and 10 mm bore orifices under conditions 2 and 5. The pressure data are measured at the end of pipeline (WE). The measured pressure waves indicate that the pipeline with 15 (β = 0.6789) or 10 mm (β = 0.4525) bore orifices is not influenced by the

restrictions. The magnitude, wavespeed, and initial drop of pressure wave are almost identical with the measured data of intact or unblocked pipe.

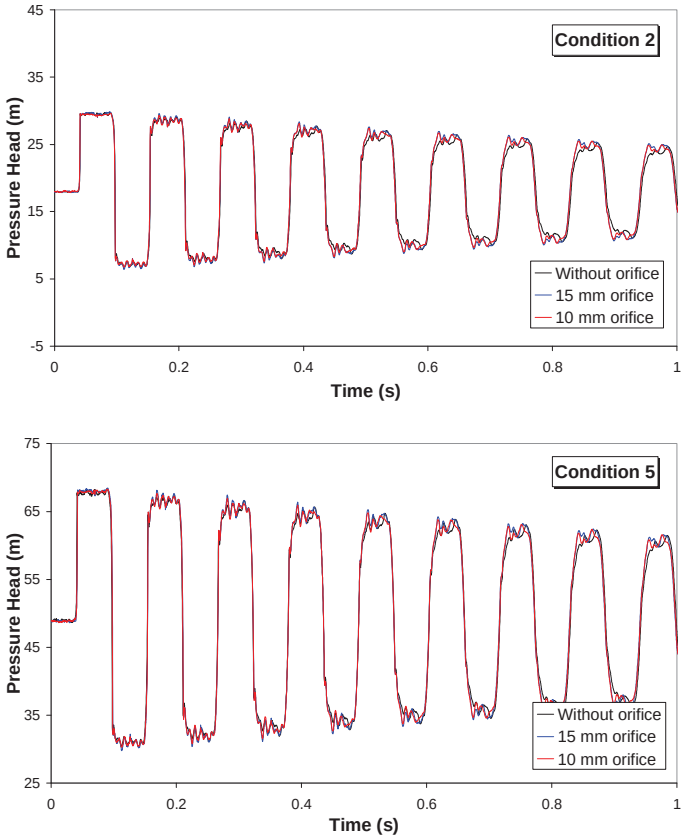

Figure 8.14 Measured Data of Pipeline with 10 and 15 mm Orifices

The measured data of orifices indicate that the additional inertia force, multiple pressure reflections, and lagging effect of pressure wave originated by the orifice are significant when the orifice bore is less than 5 mm (β = 0.2262). Pressure waves generated by fast transient events can be fully transmitted across an orifice in which the bore is larger than 5 mm. In this case, there is no significant unsteady effect by the restriction. There is slight pressure damping effect when the orifice bore is equal to 5 mm.

Fig. 8.15 shows the comparison of pressure data measured between WM and EM under the flow condition 5. As the orifice bore size decreases, the initial pressure difference between WM and EM increases and the initial pressures between WM and EM are almost same for 5 or 10 mm orifices. Although 2 and 3 mm orifices transform the pressure waves, the great part of the pressure transients generated at the WE are transmitted across the orifices. In the case of 5 and 10 mm orifices, the initial pressures and the shape of pressure waves are

almost identical because the orifices do not affect transients and the pressure waves are fully transmitted across the orifices. An orifice is important elements from the viewpoint of pipeline system design because it can adequately represent different flow system components, such as valves, blockages, leakage, and joints. Appendix E shows the measured transient data when the pipeline has a gate valve in the middle of pipeline. The pressure data are collected according to the degree of valve open and close. The measured data present the state of transmission and reflection waves by the gate valve.

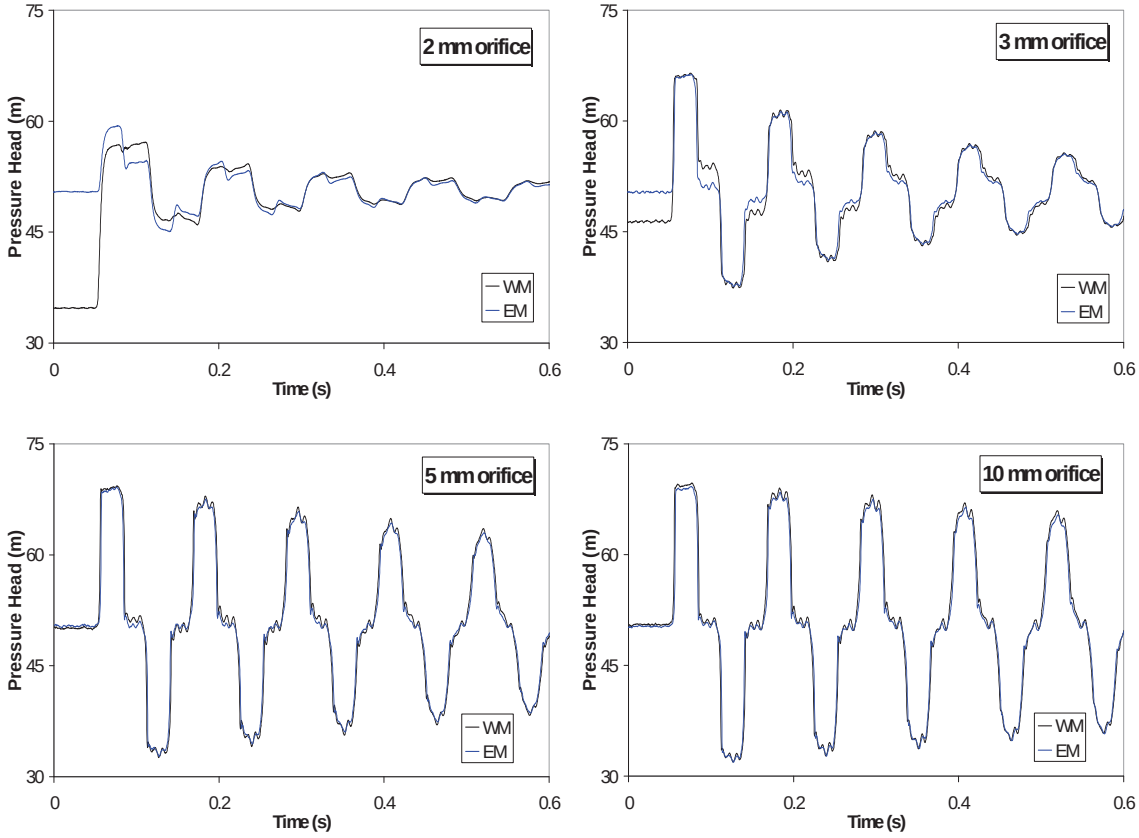

Figure 8.15 Measured Data between WM and EM

8.3.2 Measured Transient Data of Pipeline with Blockages

Figs. 8.16 and 8.17 show the comparisons between the measured pressure data of an intact (or unblocked) pipe and the measured pressure data of pipeline with 10, 5, and 3 mm bore blockages (153 mm axial length and brass blockage) under various flow conditions shown in Table 8.5. The pressure data are measured at the end of pipeline (WE) and middle of pipeline (WM). The pressure data are plotted at the same scale graphs (pressure measure time: 1 second and measured pressure head range: 70 m) to compare each pressure variation, wavespeed, and pressure wave shape during same test condition. Similar to the orifice data, there is no transient pressure trace when the pipeline has 2 mm bore blockage or less. The initial pressure drops indicate the net pressure losses across the restrictions. As the bore size decreases, the magnitude of pressure wave decreases.

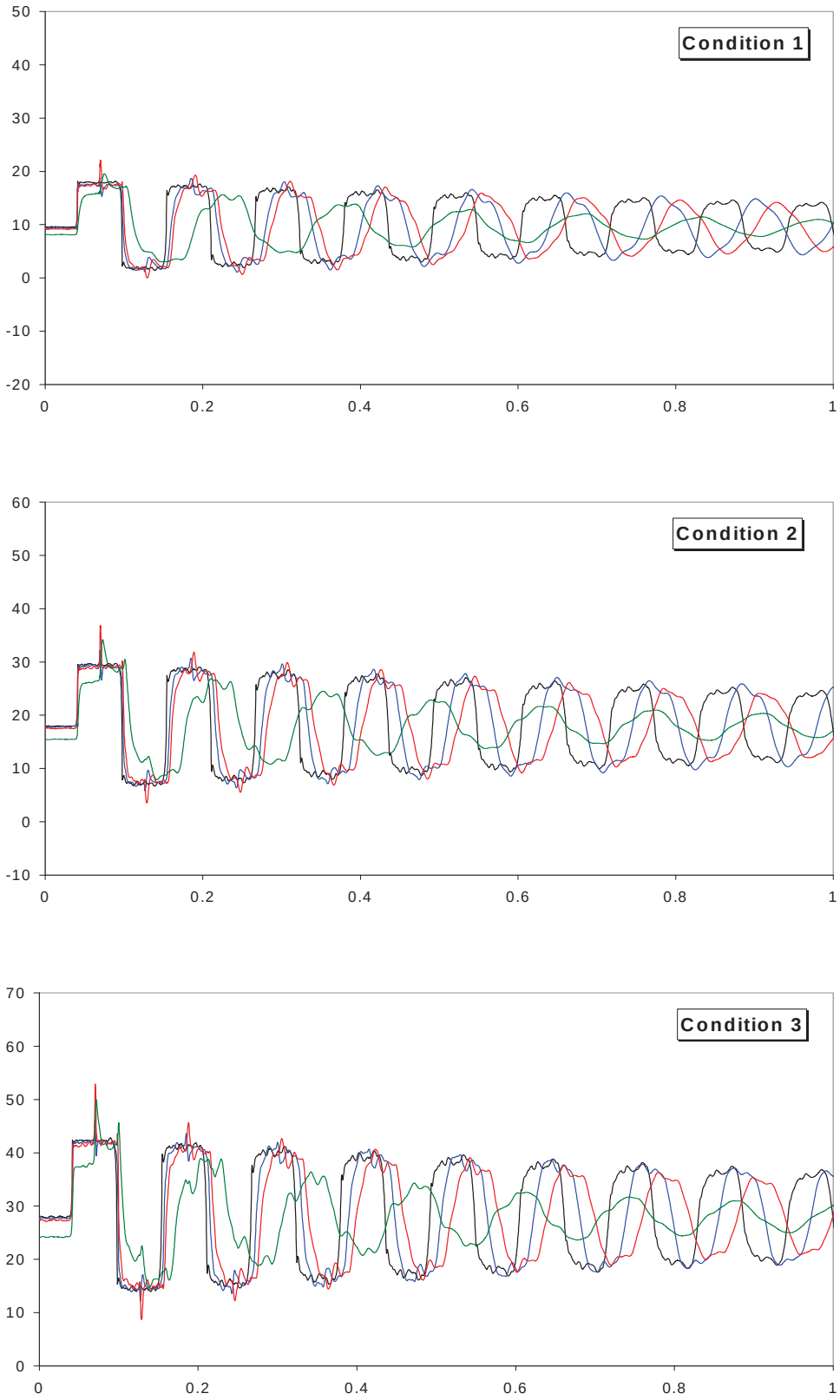

Figure 8.16 Measured Pressure Data (at WE) of Pipeline with Blockages

(The largest magnitude (black): intact or unblocked pipe, the second (blue): 10 mm blockage, the third (red): 5 mm blockage, the smallest magnitude (green): 3 mm blockage, x-axis: measurement time (s), and y-axis: pressure head (m))

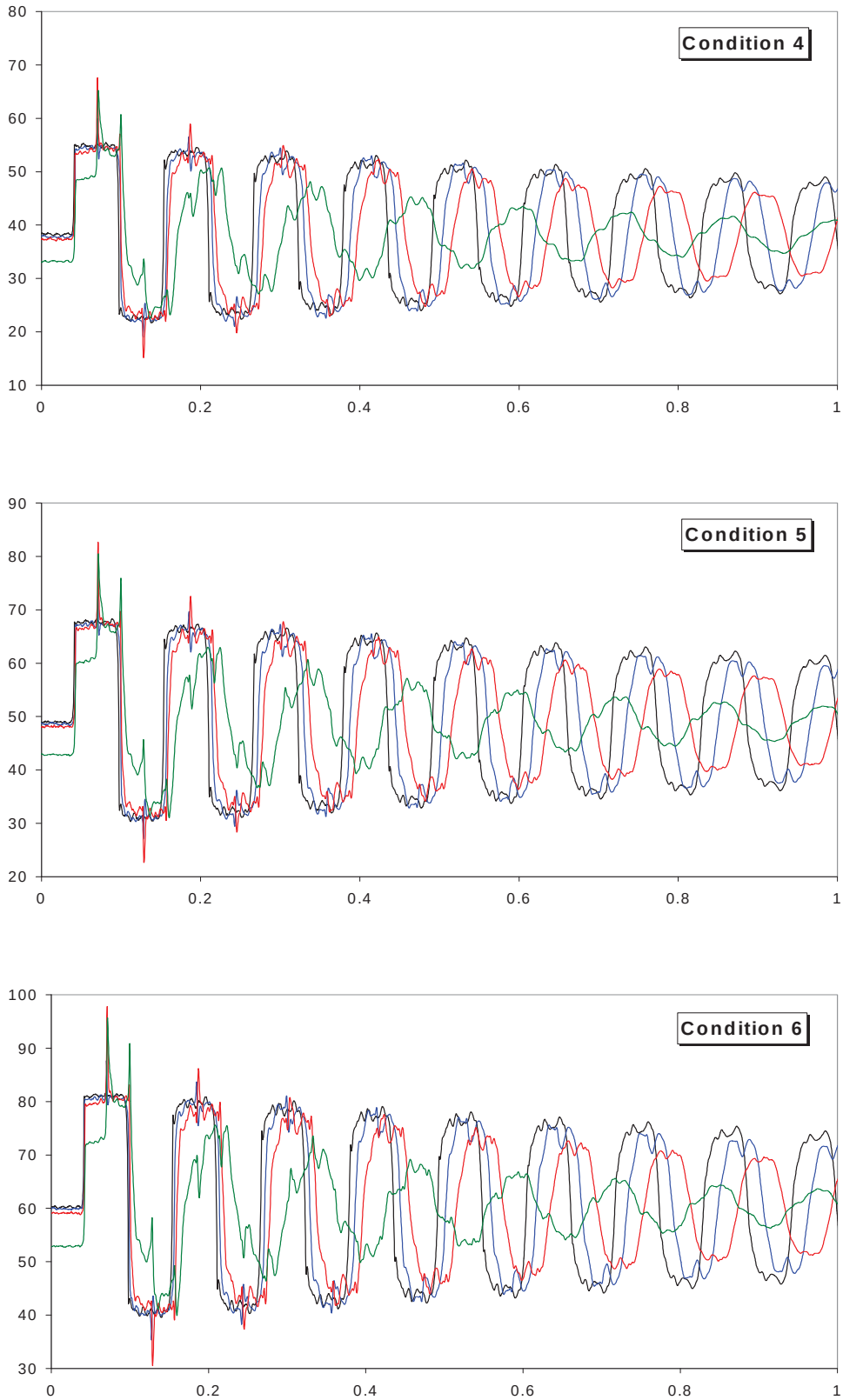

Figure 8.16 Measured Pressure Data (at WE) of Pipeline with Blockages (continued)

(The largest magnitude (black): intact or unblocked pipe, the second (blue): 10 mm blockage, the third (red): 5 mm blockage, the smallest magnitude (green): 3 mm blockage, x-axis: measurement time (s), and y-axis: pressure head (m))

Unlike the orifice data, blockages generate high frequency pressure spikes when the pressure waves encounter the blockages in the pipeline because of the change of pipe wall thickness. The wavespeed instantaneously increases when the pressure wave meets the thickened pipe wall due to the brass blockage and the amplified wavespeeds generate pressure spikes. We can characterize the location, bore size, and axial length of blockages by analysing these pressure spikes. Similar to the orifice data, the most important characteristics of the measured pressure data are the wavespeed lagging effect due to the reduction of bore size. Table 8.8 shows the wavespeeds of measured pressure waves by using the time between first and second pressure rise when the pipeline has 3, 5, or 10 mm blockages under various test conditions. The wavespeed decreases when the pipeline has a smaller bore size and a lower pressure condition.

Table 8.8 Measured Wavespeeds for 3, 5, 10 mm Blockages

	Intact Pipe (m/s)	3 mm Blockage (m/s)	5 mm Blockage (m/s)	10 mm Blockage (m/s)
Condition 1	1334.4	1042.5	1245.8	1285.8
Condition 2	1331.4	1120.2	1264.1	1299.7
Condition 3	1334.4	1161.4	1274.9	1305.3
Condition 4	1331.4	1186.7	1285.8	1307.4
Condition 5	1331.4	1203.3	1296.9	1311.0
Condition 6	1334.4	1215.5	1297.3	1311.0

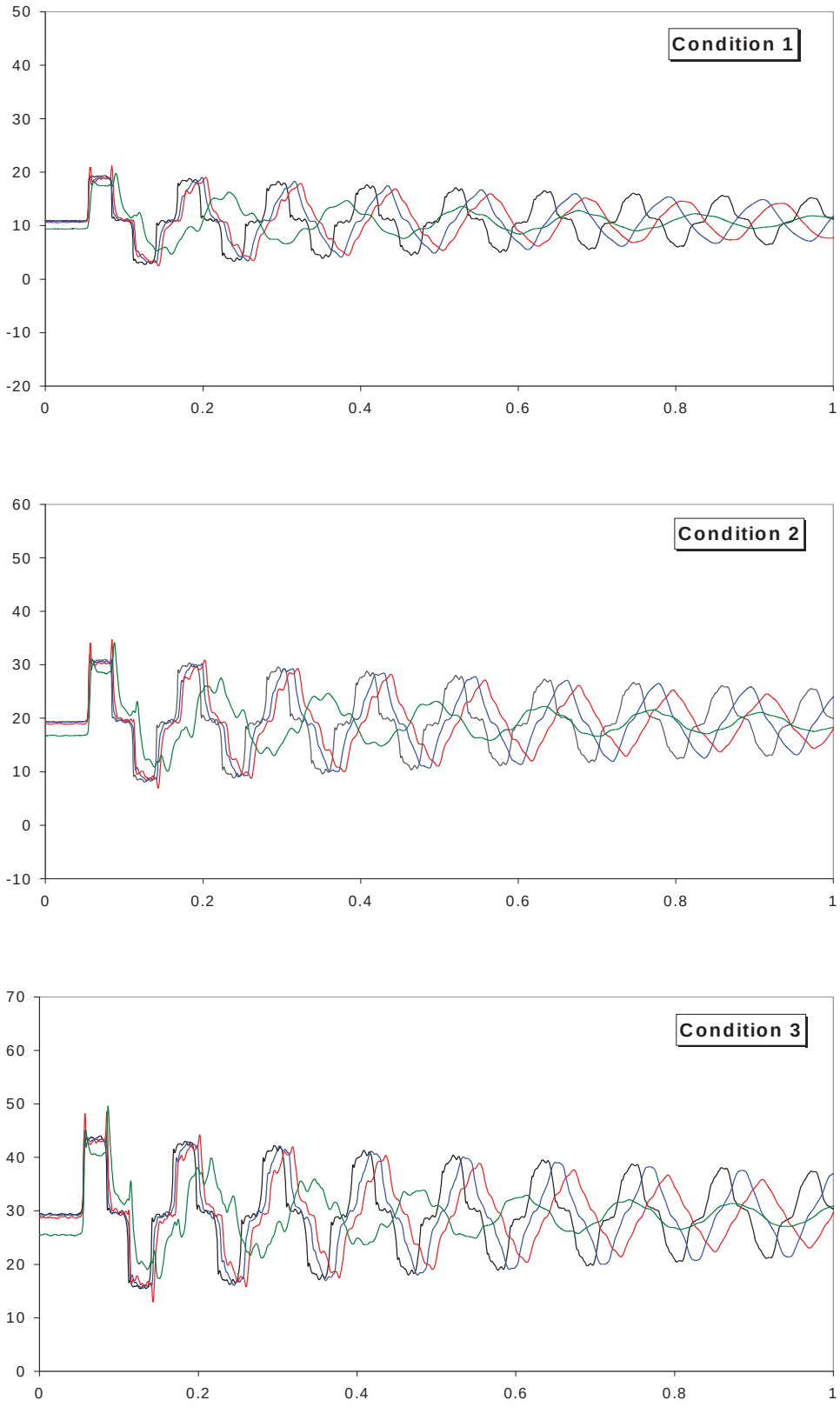

Figure 8.17 Measured Pressure Data (at WM) of Pipeline with Blockages

(The largest magnitude (black): intact or unblocked pipe, the second (blue): 10 mm blockage, the third (red): 5 mm blockage, the smallest magnitude (green): 3 mm blockage, x-axis: measurement time (s), and y-axis: pressure head (m))

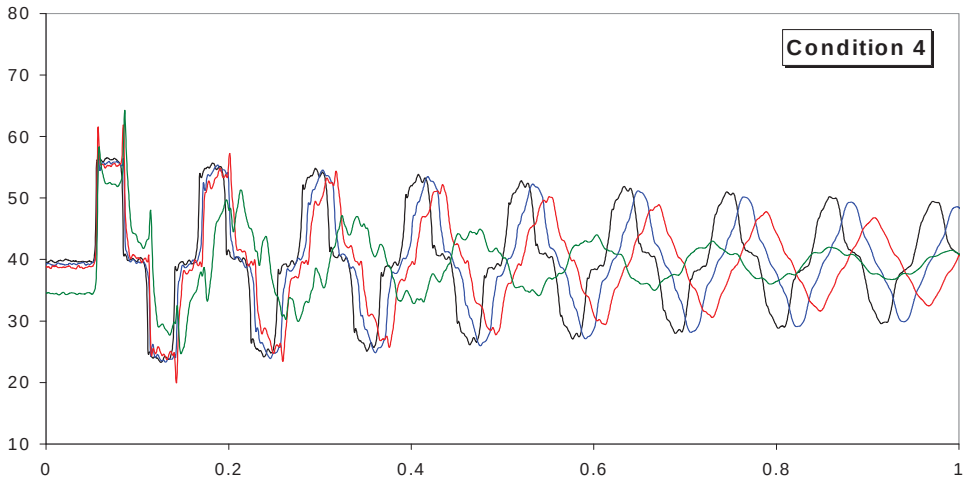

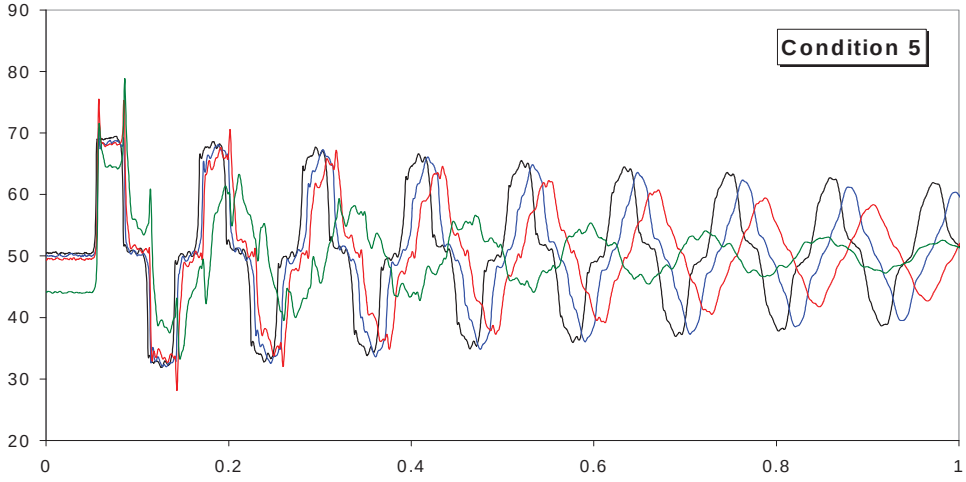

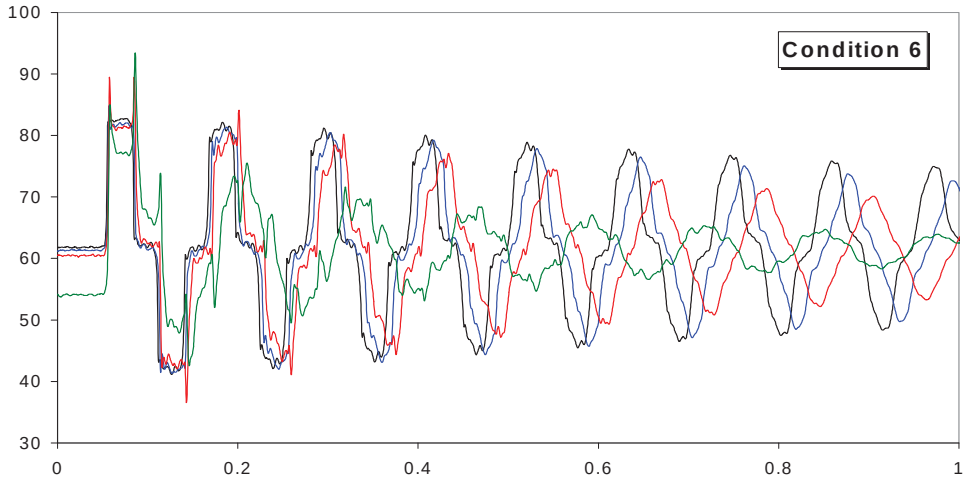

Figure 8.17 Measured Pressure Data (at WM) of Pipeline with Blockages (continued)

(The largest magnitude (black): intact or unblocked pipe, the second (blue): 10 mm blockage, the third (red): 5 mm blockage, the smallest magnitude (green): 3 mm blockage, x-axis: measurement time (s), and y-axis: pressure head (m))

8.3.3 Comparison between Measured Orifice and Blockage Data

Fig. 8.18 shows the comparison of measured data between a 3 mm orifice and a 3 mm blockage and between a 5 mm orifice and a 5 mm blockage under the flow condition 5. The blockage data clearly present pressure spikes when compared to orifice data and the lagging effect of pressure wave is more significant in the measured blockage data because of the additional inertia effect of axial-extended length.

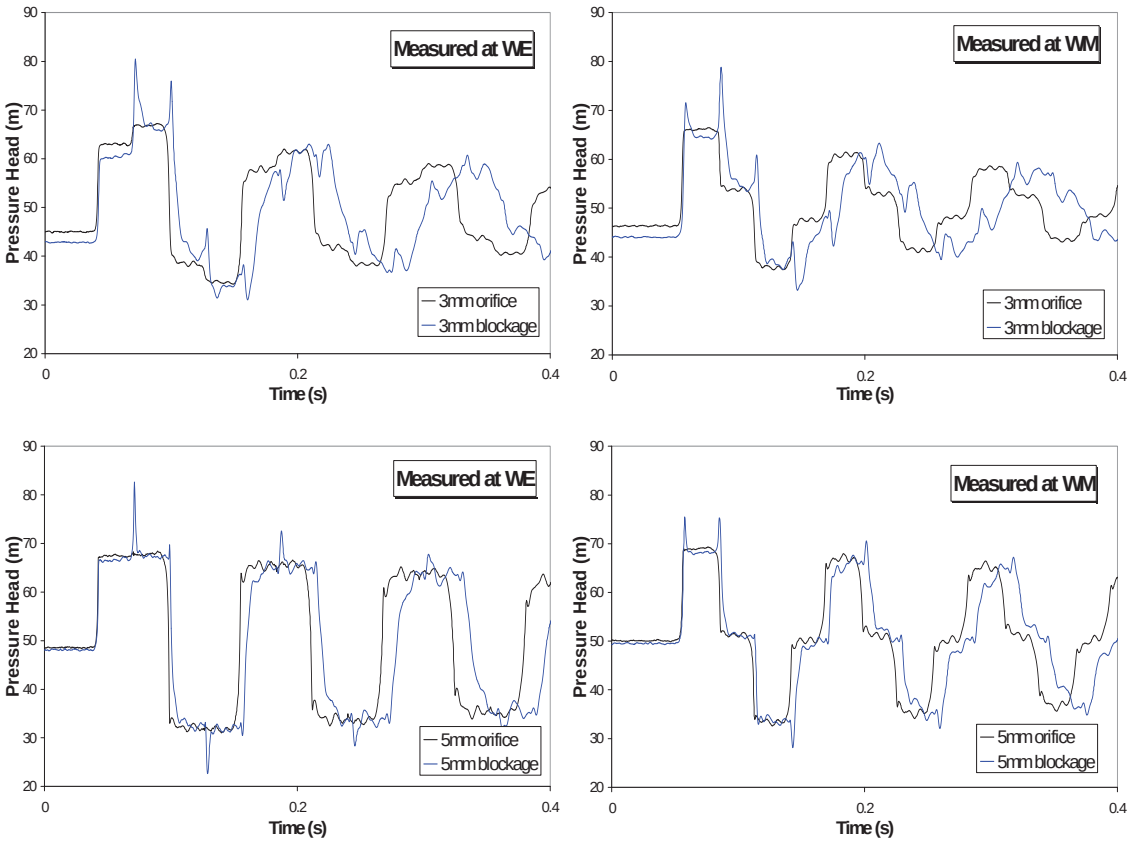

Figure 8.18 Comparison of Measurements between Orifices and Blockages

8.3.4 Measured Transient Data of Pipeline with Soft Blockages

Fig. 8.19 shows the comparison of measured transient data for a hard material blockage (brass, Young's modulus E = 103.4 GPa) and a soft material blockage (silicon, E = 37.5 kPa). The solidity of natural blockages formed by solid deposition or pipe wall corrosion usually softens when compared to the pipe wall materials. Also, the surface of natural blockage is rough and has irregular shape (see Appendix F about the effect of rough wall blockage during transients). For these natural blockage tests during transients, soft

blockage elements have been made of silicon. The outside of blockage is the same as the copper pipe presented in the Chapter 4. The inside of the copper pipe is filled up by silicon. A drill was used to bore the hardened silicon. Fig. 8.19 (a), (b), and (c) show the measured pressure data according to the bore size under the test condition 2. The test results are similar to the measured data when the pipeline has an air pocket presented in Chapter 7. A gas cavity can be considered as a spring or cushion loaded with the liquid. A pressure pulse compresses the spring during transients, so the cavity greatly reduces the wavespeed and the magnitude of pressure wave. The effect of pressure damping is more serious, if the volume of cavity is bigger. The soft blockage has a similar mechanism to that of a gas cavity. Soft material also can be considered as a cushion that reduces the wavespeed and the amplitude of pressure wave during transient events. Fig. 8.19 indicates that the effects of wavespeed delay and the pressure damping is more significant, as the pipeline has a larger soft blockage (larger soft material and smaller blockage bore size). Also, naturally the influence of the cushion effect by a gas cavity or a soft material is most significant for low pressurised systems. The initial size of a soft blockage is more contracted by higher initial pressure condition, therefore the actual size of soft blockage in the high pressure condition is smaller than that in the low pressure condition. In the Fig. 8.19 (d), the speed of pressure wave is faster and the damping effect of pressure wave by 5 mm blockage is less when compared to the result of the Fig. 8.19 (a). The upward or downward spike of the first pressure rise indicates the location of a blockage. The upward spike (sudden pressure rise) is generated by the abrupt increase of wavespeed when the pressure wave meets the hard-material blockage, while the downward spike is generated by the decrease of wavespeed when the pressure wave meets the soft-material blockage.

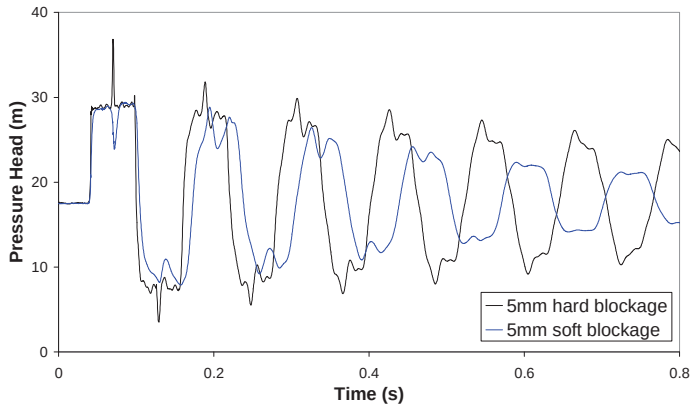

(a) Measured Data with 5 mm Blockage (condition 2)

Figure 8.19 Comparison of Measurements between Hard and Soft Blockages

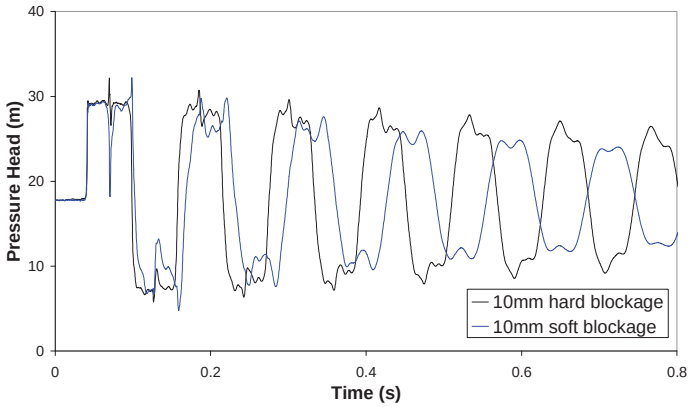

(b) Measured Data with 10 mm Blockage (condition 2)

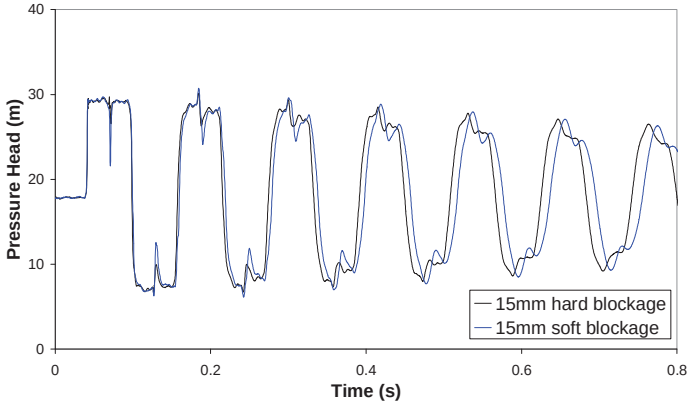

(c) Measured Data with 15 mm Blockage (condition 2)

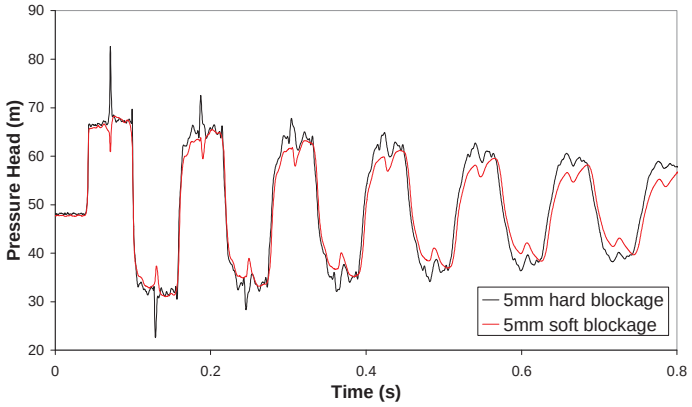

(d) Measured Data with 5 mm Blockage (condition 5)

Figure 8.19 Comparison of Measurements between Hard and Soft Blockages (continued)

8.3.5 Measured Transient Data in Gas Pipeline with Orifices and Blockages

Laboratory experiments have been carried out for the investigation of unsteady orifice and blockage flows in the gas pipeline. Dry air (25.4^{o}C) supplied by air compressor was used as the fluid medium. Transient events were generated by the fast closure of a flow control valve at WE. Pressures and temperatures were monitored at 4 points (WE, WM, EM, EE) at brass blocks along the pipeline and at the bottom of both tanks. The sampling frequency of measured data is 4 kHz. Table 8.9 shows the initial flow conditions and the wavespeeds computed by using the time between first and second pressure rise.

Table 8.9 Wavespeeds and Initial Flow Conditions

	Wavespeed (m/s)	Velocity (m/s)	Reynolds Number	Initial Pressure (kPa)
Intact Pipe	346.7	37.54	53,181	300.3
15 mm Orifice	347.5	29.80	42,216	228.2
15 mm Blockage	346.6	29.75	42,145	236.9
10 mm Orifice	345.8	25.84	36,606	227.3
10 mm Blockage	342.7	29.55	41,862	220.0

Figs. 8.20 and 8.21 show the measured transient data when the gas pipeline has orifices and blockages with 10 and 15 mm bores. There is no transmitted transient pressure trace when the pipeline has 5 mm bore restriction or less because the small bore restriction completely mitigates the pressure variation of transients. Unlike the measured data of orifices and blockages for water transients, the shapes of pressure waves affected by orifices and blockages are much similar to each other when compared to the measured data between 15 mm orifice and 15 mm blockage or between 10 mm orifice and 10 mm blockage because the inertial effect in the compressible flow is much less than that of incompressible flow.

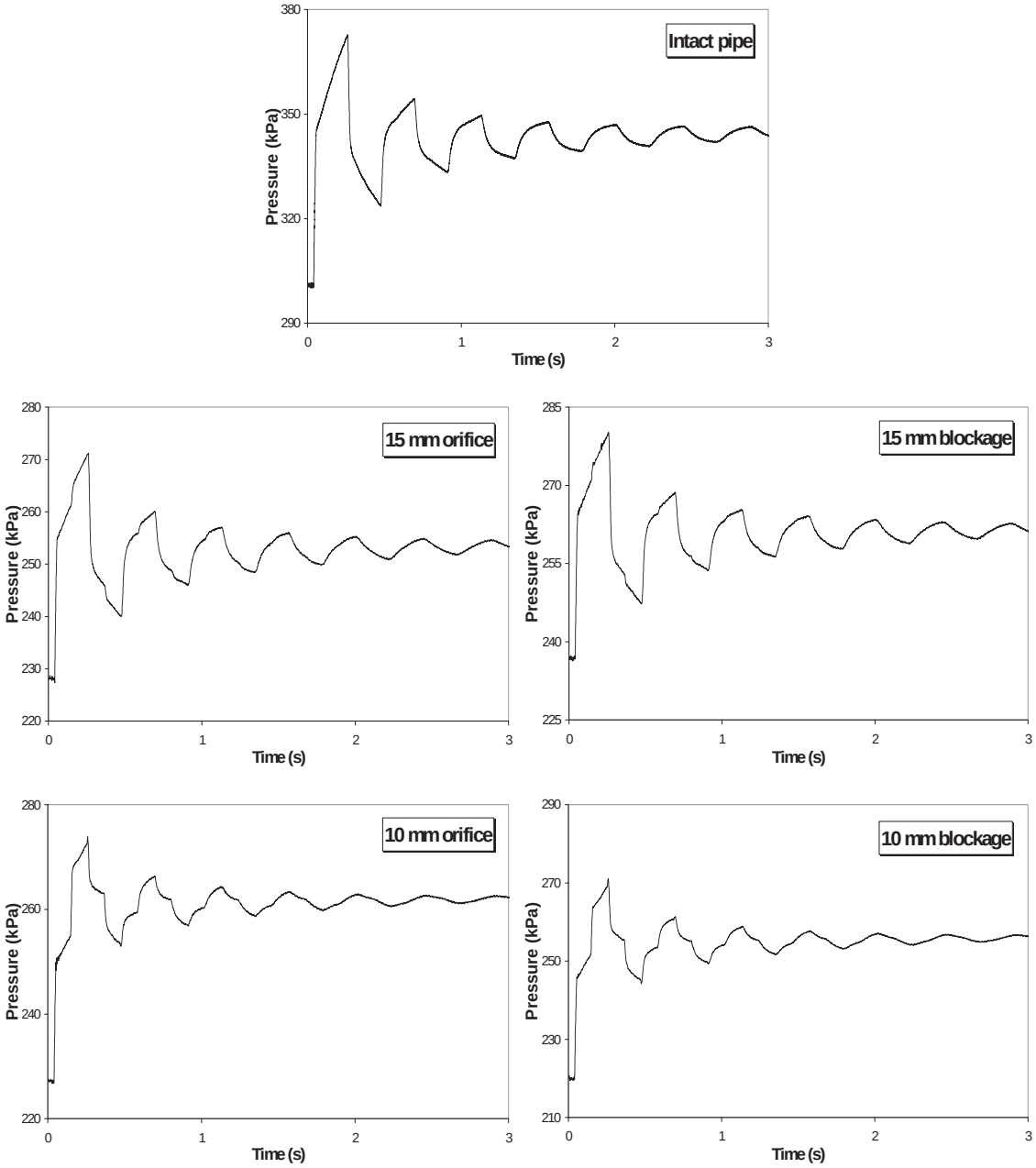

Figure 8.20 Measured Data in Gas Pipeline with Orifices and Blockages (WE)

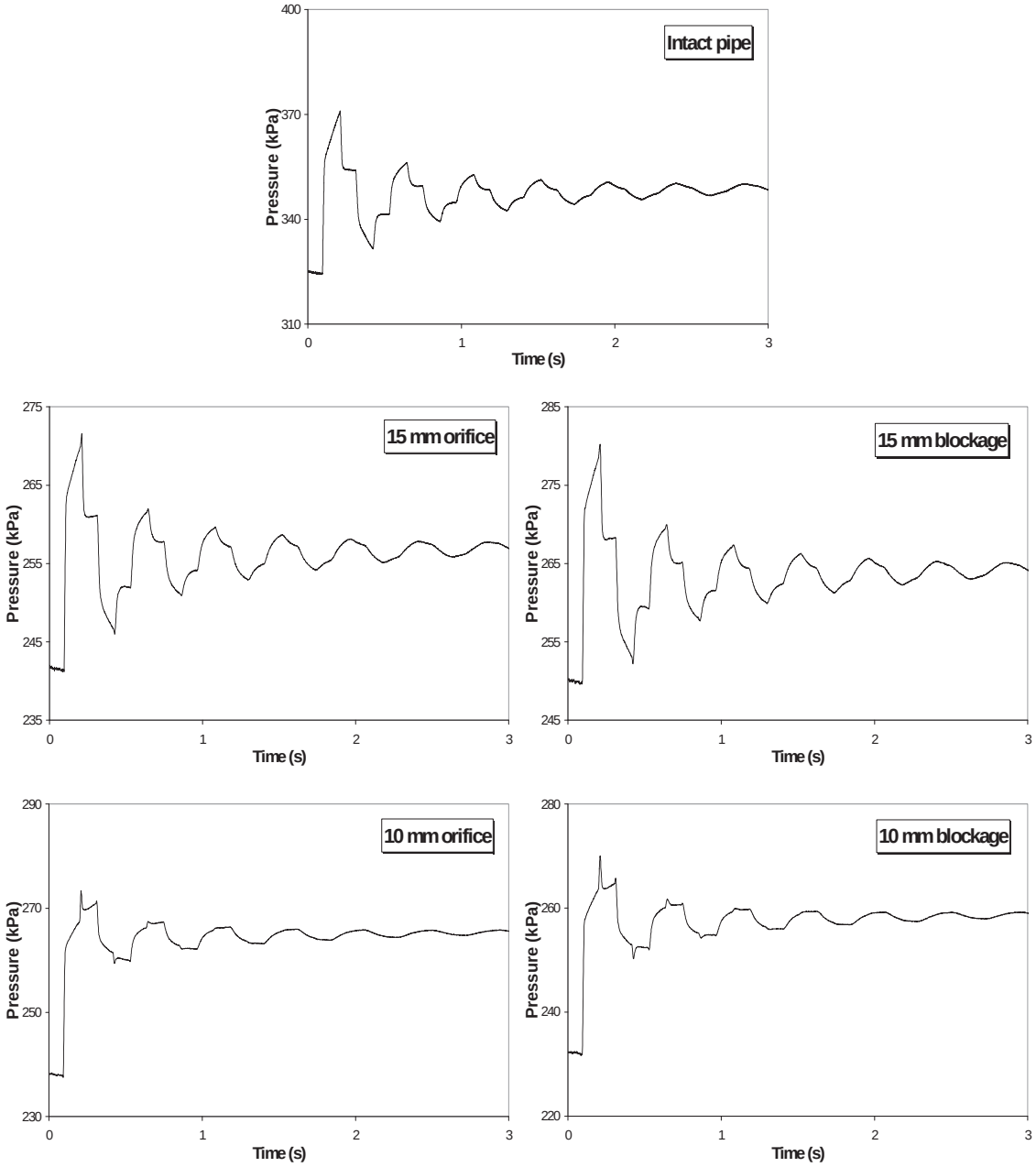

Figure 8.21 Measured Data in Gas Pipeline with Orifices and Blockages (WM)

8.4 NUMERICAL INVESTIGATION FOR THE PROPOSED MODELS

Numerical experiments have been executed for verifying the proposed models and for investigating the dynamic behaviour of transient pipe flows with the various orifices and blockages. The pipeline system shown in Fig. 8.22 has been used for numerical experiments. This system is identical with the laboratory pipeline system used for experimental verification. Transient events are generated by an instantaneous valve closure.

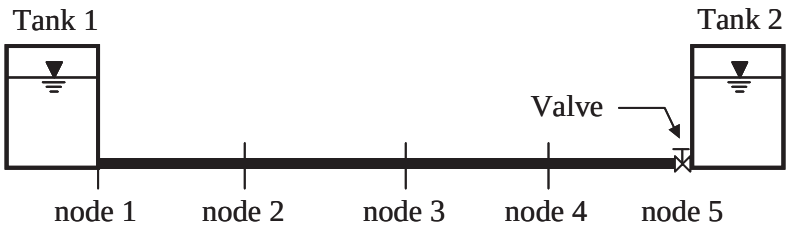

Figure 8.22 Pipeline System for Numerical Experiments

Fig. 8.23 shows pressure wave traces at 4 different nodes (node 2, 3, and 4 that divide the pipe into equal lengths) according to the change of the location of 2.5 mm orifice (β = 0.113). The initial flow velocity is 0.142 m/s with a Reynolds number of 3,128. A steady orifice model has been used for these simulations. The change of orifice location has a big effect on the pressure wave by transients. Pressure waves show a different shape and magnitude according to the locations of measured node and orifice. These characteristics can be used for detecting the locations of partially or fully closed system components due to operator error in a pipeline system.

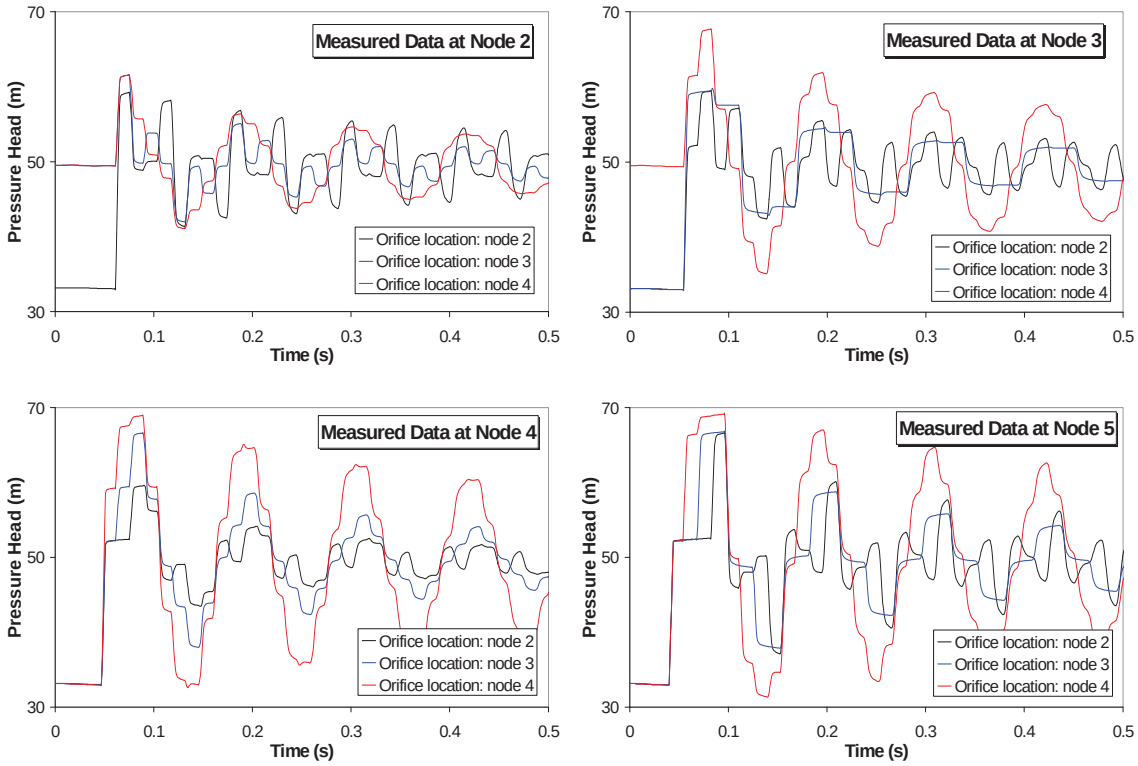

Figure 8.23 Pressure Waves for a Change of Orifice Location

Fig. 8.24 shows the comparison of numerical simulations of steady blockage model when the pipeline has 3 different lengths of brass blockage (axial-extended orifice) at the middle of pipeline. The bore size of these blockages is 3 mm and the axial lengths are 0.153, 0.938, and 1.876 m respectively. The pressure waves are measured at the node 5. As the blockage length increases, the magnitude and wavespeed of pressure wave dramatically decrease and pressure wave appears more complex effects due to the multiple pressure reflections.

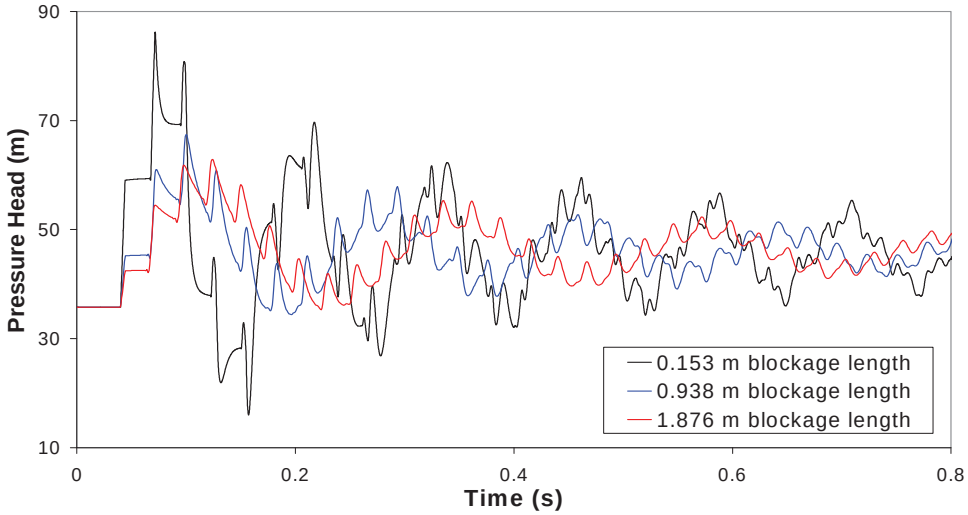

Figure 8.24 Pressure Waves according to the Length of Blockage

Fig. 8.25 shows the comparisons of simulation results between the steady orifice model and the instantaneous inertia model when the pipeline has a 2.5 mm orifice (β = 0.113) at the node 3. The initial flow velocity is 0.142 m/s with a Reynolds number of 3,128. The results of instantaneous inertia model are almost identical with the results of steady orifice model.

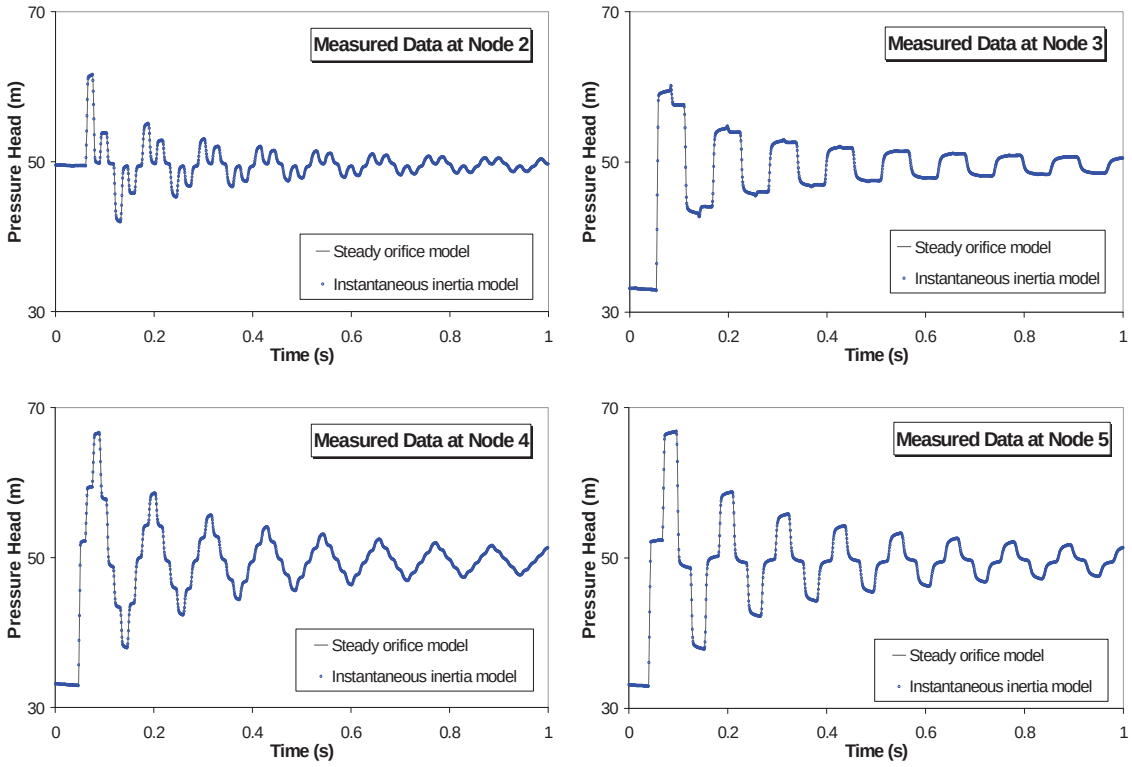

Figure 8.25 Comparison of Steady Orifice and Instantaneous Inertia Models

For the same test condition with a 2.5 mm orifice, Fig. 8.26 shows the comparisons of simulation results between the steady orifice model and the frequency-dependent model. Unlike the results of the instantaneous inertia model, the results of the frequency-dependent model show additional pressure wave attenuation and a wave dispersion effect.

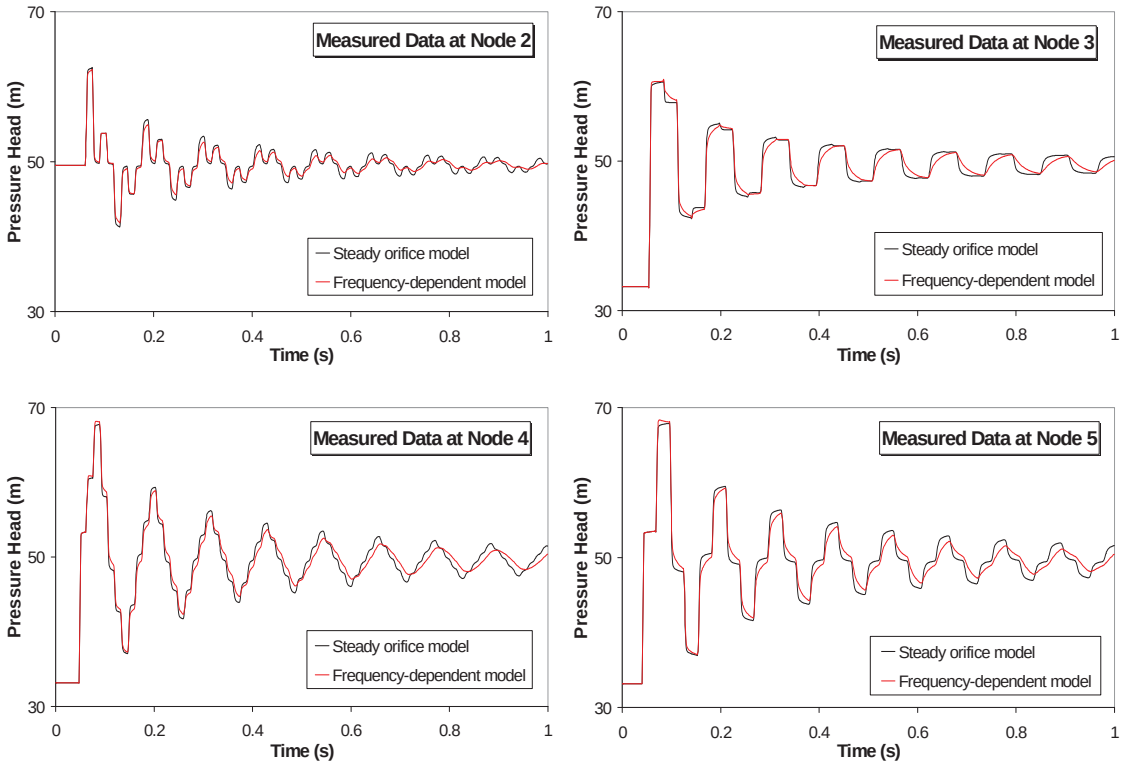

Figure 8.26 Comparison of Steady and Frequency-Dependent Models

Fig. 8.27 shows the comparisons of simulation results between the steady blockage model and the instantaneous inertia model when the pipeline has a 3 mm blockage (153 mm axial length) at the middle of pipeline. The initial flow velocity is 0.169 m/s with a Reynolds number of 3,723. Similar to the results for orifice flow shown in Fig. 8.25, the results of the instantaneous inertia model are almost identical with the results of the steady orifice model.

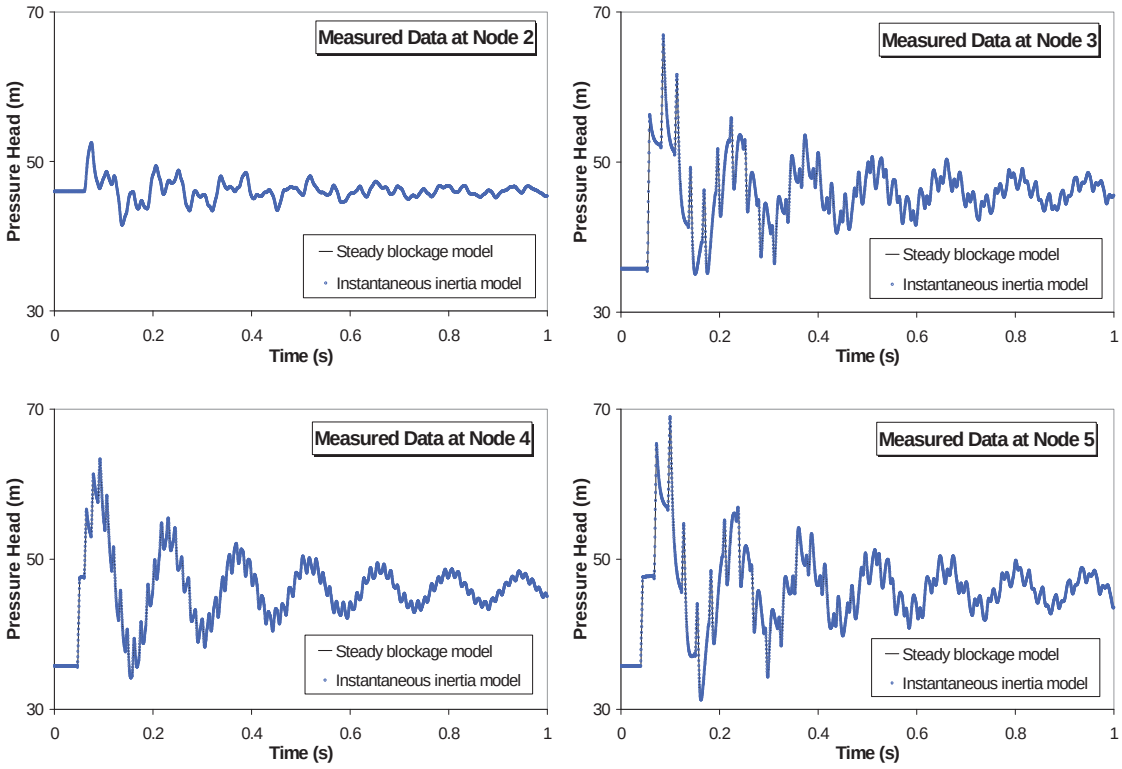

Figure 8.27 Comparison of Steady Blockage and Instantaneous Inertia Models

For the same test condition with 3 mm blockage (153 mm axial length), Fig. 8.28 shows the comparisons of the simulation results between the steady blockage model and the frequency-dependent model. Similar to the results of Fig. 8.26, the results of the frequency-dependent model shows additional pressure wave damping and a wave dispersion effect.

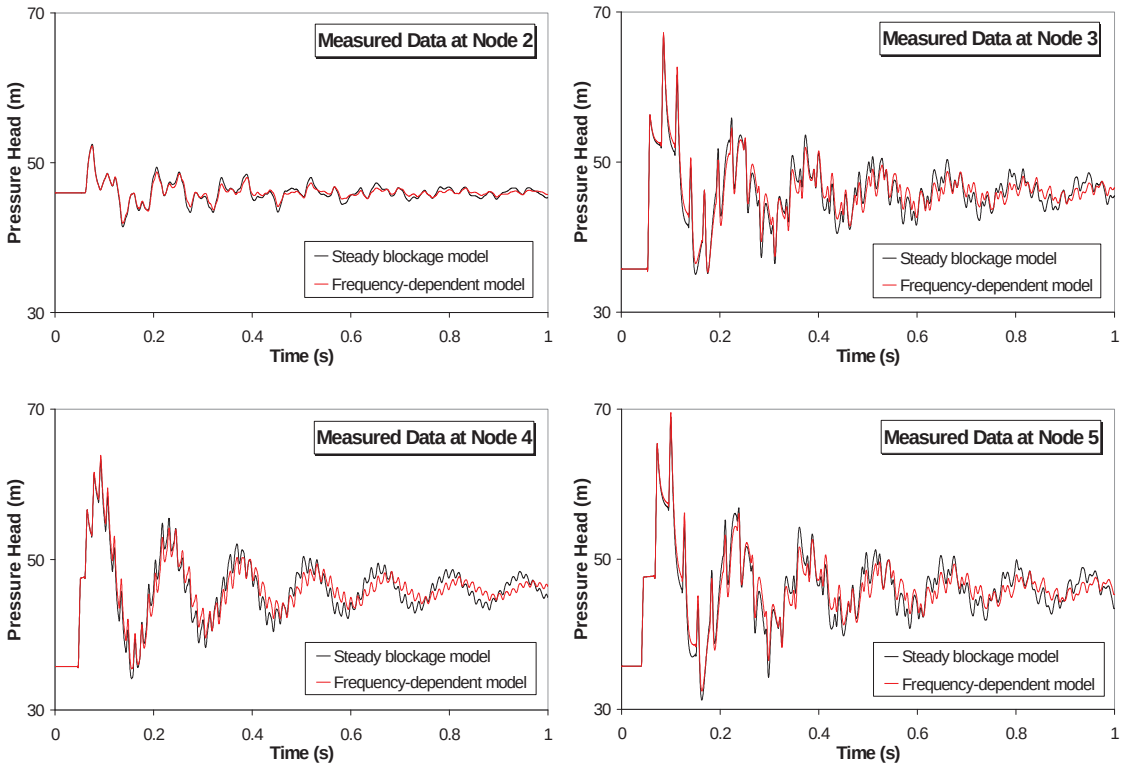

Figure 8.28 Comparison of Steady and Frequency-Dependent Models

The results of the instantaneous inertia models for an orifice and a blockage in Figs. 8.25 and 8.27 indicate the time dependent description [Funk et al., 1972] of the dynamic response of orifices and very short lines based on accelerating and decelerating flow does not provide additional energy dissipation or dispersion when their results are compared with the results of steady state model. As a result, this research will not use the instantaneous inertia model but ratter will use the frequency dependent model for the following simulations using the measured data of orifices and blockages.

8.5 SIMULATION RESULTS FOR ORIFICES AND BLOCKAGES

Figs. 8.29 and 8.30 show the comparison between measured pressure data and simulation results based on the proposed frequency-dependent model for test condition 5 when the pipeline has 2, 3, 5, and 10 mm orifices at the mid-point of pipeline. Pressure data for measurement at the end (WE) and middle (WM) of pipeline are shown in Figs. 8.11 and 8.12. The thick gray lines are the measured data, the blue and red lines are the simulation results based on the conservative solution scheme including a steady orifice model and a frequency-dependent model respectively.

The simulation results for both the steady orifice and the frequency-dependent models show good agreement in both magnitude and shape of transient pressure data. The results of the frequency-dependent unsteady minor loss model cause a slight damping and dispersion of travelling pressure wave when compared to the results of the steady orifice model and both results are almost the same for the 10 mm orifice simulation. The results seem to support the validity of the traditional view that characteristics of an unsteady orifice flow can be approximately represented by those of a steady state one. Although both the steady or unsteady models in these test cases is able to adequately represent the magnitude and shape of pressure wave, the results clearly demonstrate that the major unsteady phenomena for orifices of smaller diameter exhibits significant lagging of the wave due to the eddy inertia effect of turbulent jet flow. In particular, the discrepancy of wavespeeds between simulation results and measured data is significant when the orifice bore is less than 5 mm.

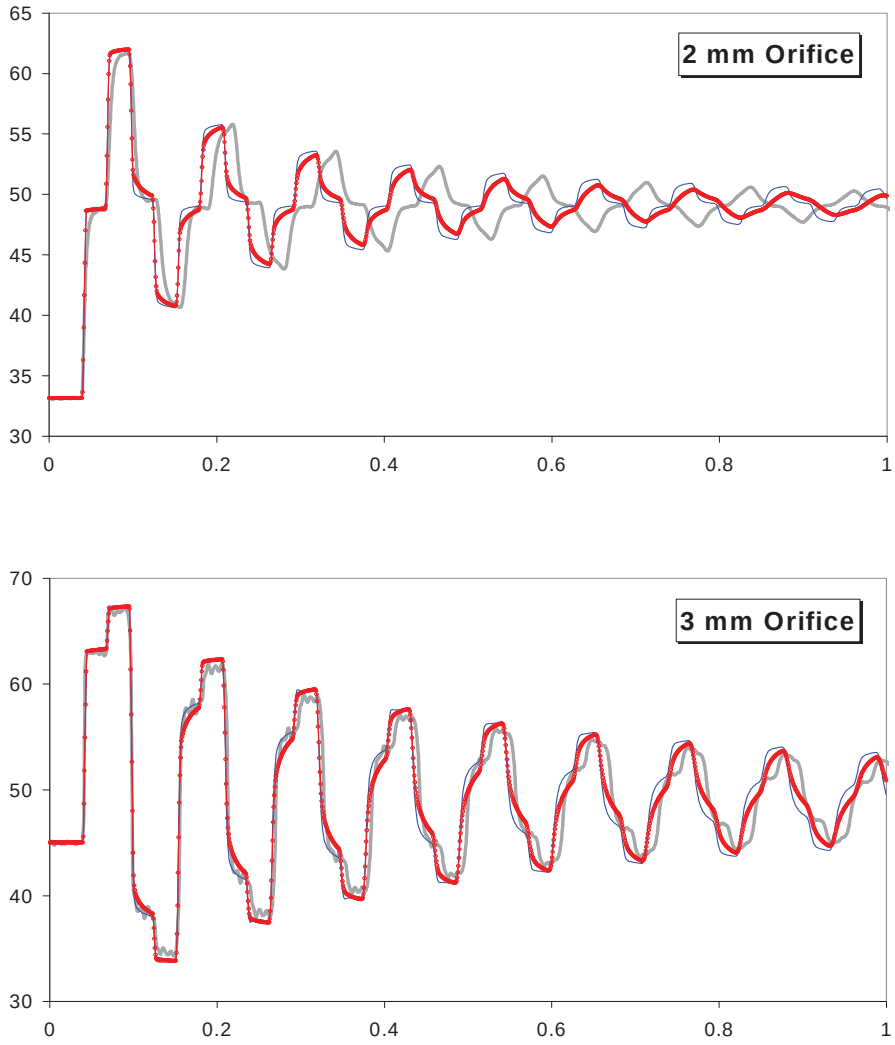

Figure 8.29 Comparison of Measured Data and Simulation Results for the Frequency-Dependent Model at the WE under the Test Condition 5

(The thick gray line: measured data, the blue line: steady orifice model, the red line: frequency-dependent model, x-axis: measurement time (s), and y-axis: pressure head (m))

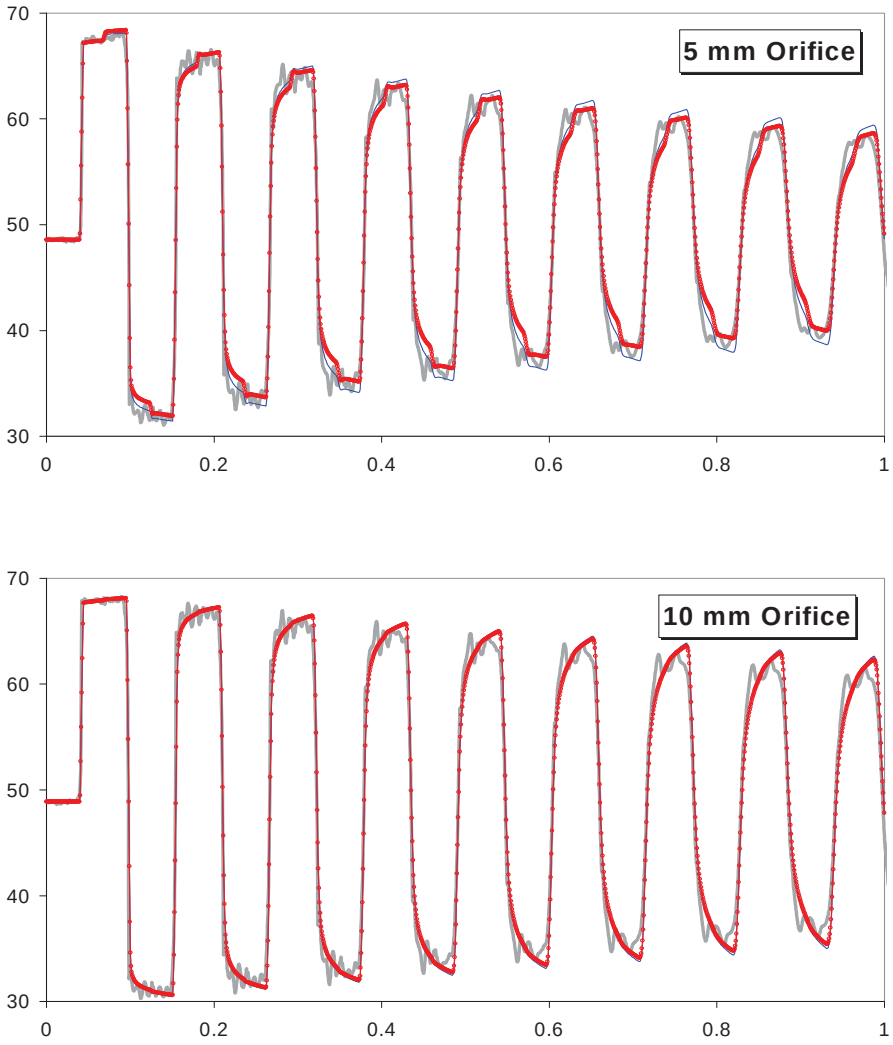

Figure 8.29 Comparison of Measured Data and Simulation Results for the Frequency-Dependent Model at the WE under the Test Condition 5 (continued)

(The thick gray line: measured data, the blue line: steady orifice model, the red line: frequency-dependent model, x-axis: measurement time (s), and y-axis: pressure head (m))

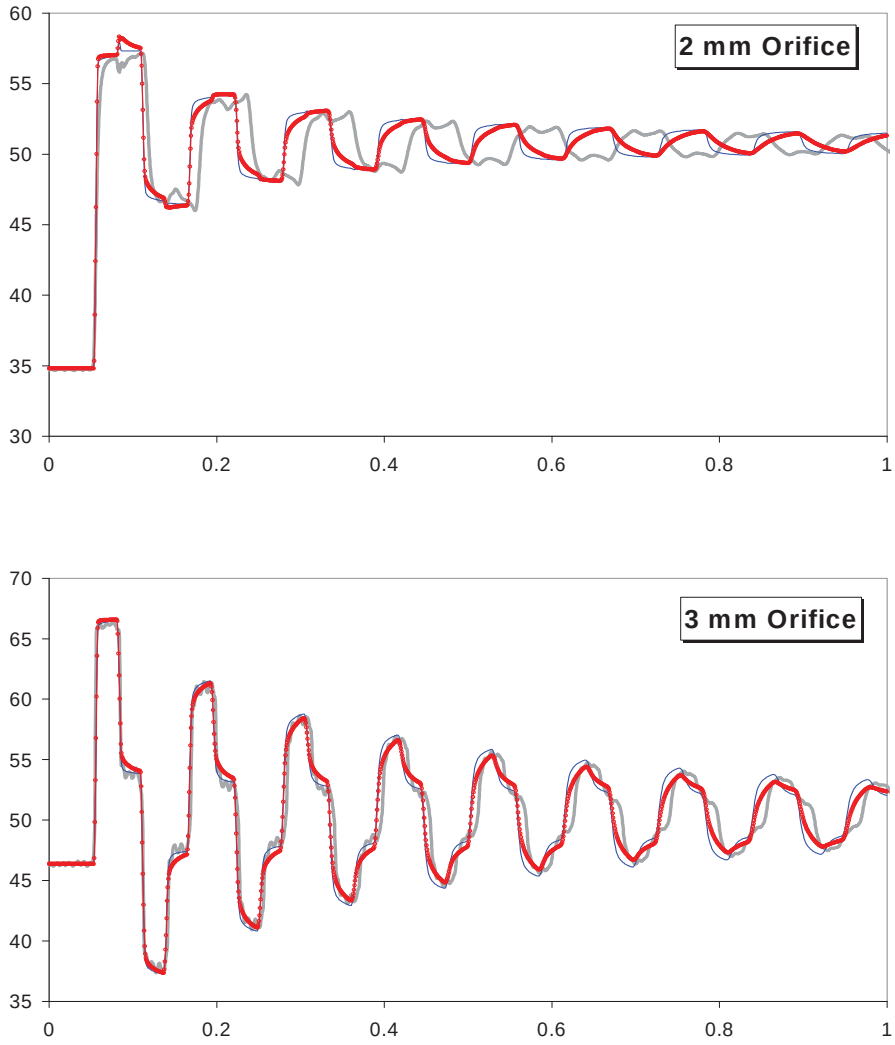

Figure 8.30 Comparison of Measured Data and Simulation Results for the Frequency-Dependent model at the WM under the Test Condition 5

(The thick gray line: measured data, the blue line: steady orifice model, the red line: frequency-dependent model, x-axis: measurement time (s), and y-axis: pressure head (m))

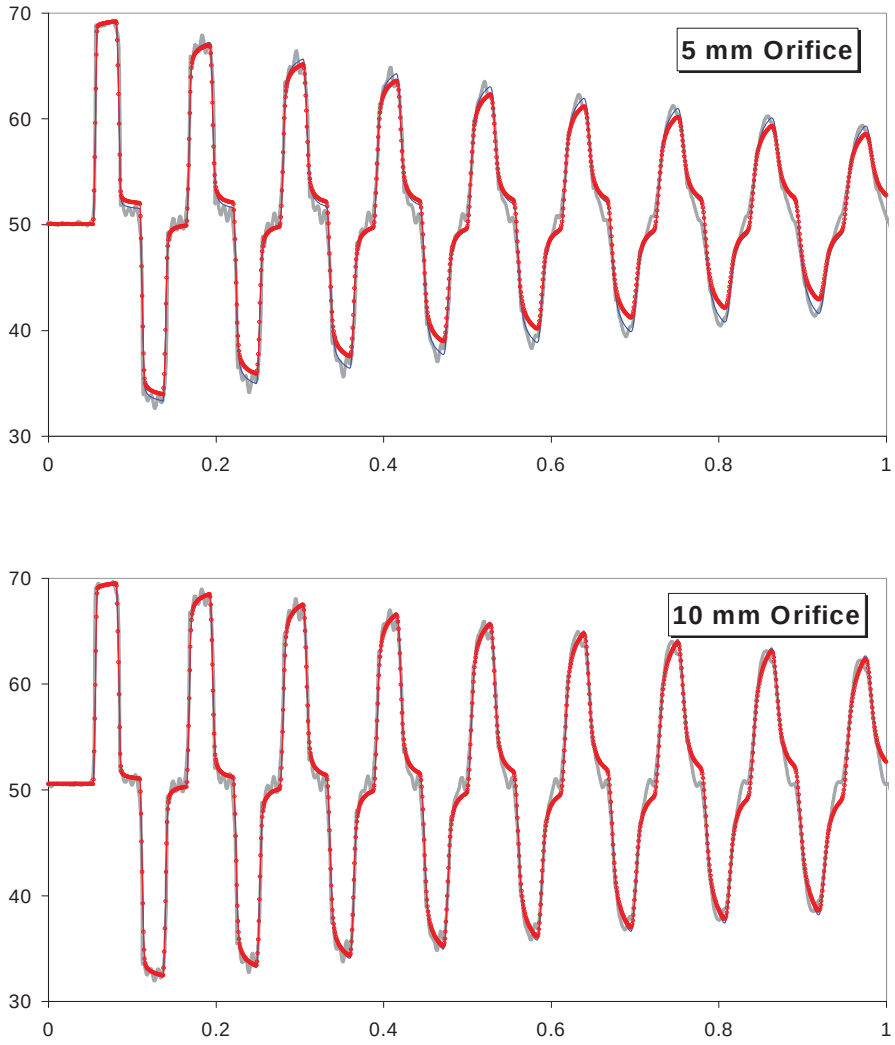

Figure 8.30 Comparison of Measured Data and Simulation Results for the Frequency-Dependent model at the WM under the Test Condition 5 (continued)

(The thick gray line: measured data, the blue line: steady orifice model, the red line: frequency-dependent model, x-axis: measurement time (s), and y-axis: pressure head (m))

Figs. 8.31 and 8.32 show the comparison between measured pressure data and simulation results for the proposed frequency-dependent model under test condition 5 when the pipeline has 3, 5, 10, and 15 mm bore blockages (153 mm axial length and brass blockage) at the mid-point of the pipeline. Pressure data for measurement at the end (WE) and middle (WM) of pipeline are shown in Figs. 8.16 and 8.17. The thick gray lines are the measured data, the blue and red lines are the simulation results based on the conservative solution scheme including a steady orifice model and a frequency-dependent model respectively.

Similar to the results for orifices, the simulation results for both the steady blockage and the frequency-dependent models show good agreement in both magnitude and shape of transient pressure data. The effects in the frequency-dependent model present slight pressure damping and dispersion when compared to the results of the steady orifice model and both results are similar for the 10 and 15 mm orifice simulations. This characteristic is similar to the results of unsteady friction models presented in Chapter 5. However, similar to the result of orifice tests, the results clearly demonstrate that the unsteady phenomena for blockages of smaller diameter exhibit significant lagging of the pressure. The proposed unsteady minor loss model cannot calculate the wave delay effect because the model is derived from the kinetic pressure difference due to instantaneous flow acceleration and deceleration at the restriction. The eddy inertia of turbulent jet flow causes the pressure wave lagging effect.

When the jet flow through the restrictions enters the sudden downstream enlargement, an intense shear layer is created along the boundary between the jet and the surrounding separation region. The high velocity in the shear layer generates turbulent eddies. The pressure inside eddies is significantly less because of its high rotational speed. This low-pressure process by the high rotational speed may cause cavitations and gas release from a fluid. Therefore, the large pressure drop due to the turbulent eddies can reduce the velocity of pressure propagation. Eddies repeat the cycle of development and reduction and the variation of eddies lags behind the flow rate transition. It is complex and difficult to develop an exact model of the eddy inertia effect for analysing the lagging effect of the pressure. The following section presents an alternative approach to adjust the pressure wave delay effect by simple wavespeed adjustment.

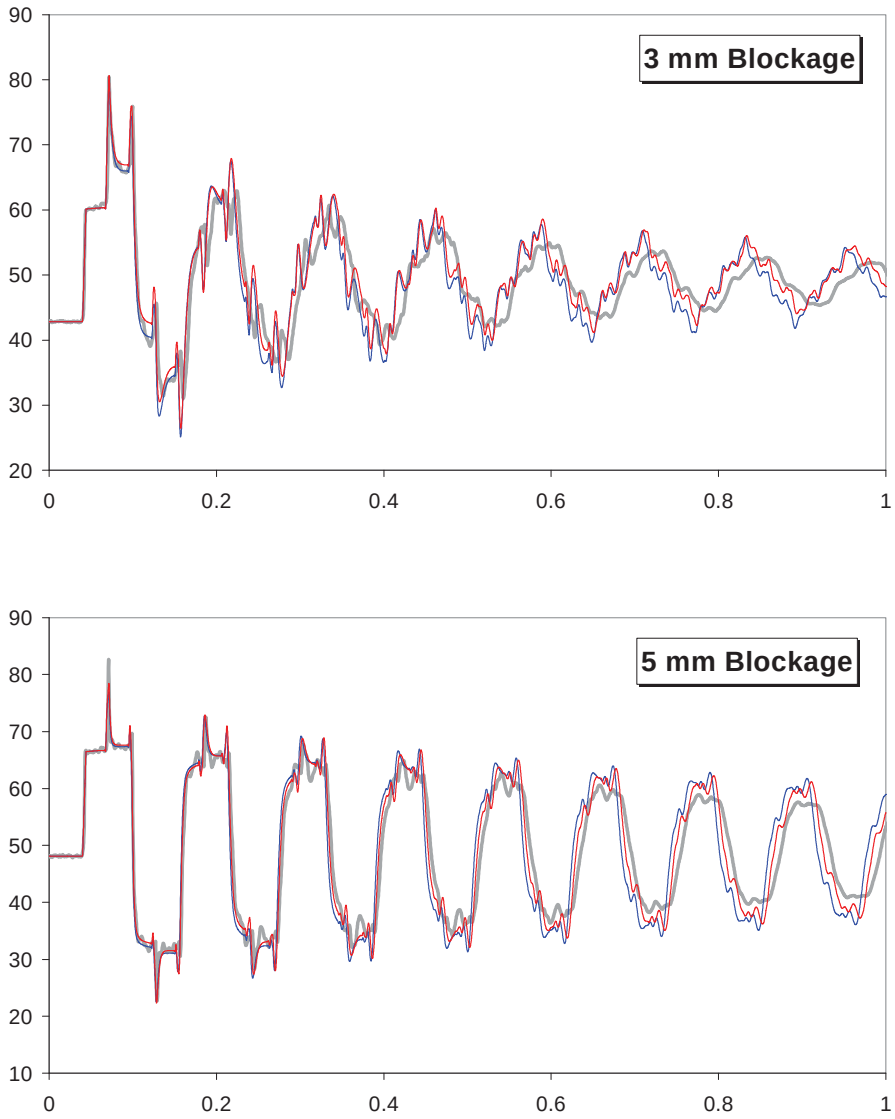

Figure 8.31 Comparison of Measured Data and Simulation Results for the Frequency-Dependent model at the WE under the Test Condition 5

(The thick gray line: measured data, the blue line: steady blockage model, the red line: frequency-dependent model, x-axis: measurement time (s), and y-axis: pressure head (m))

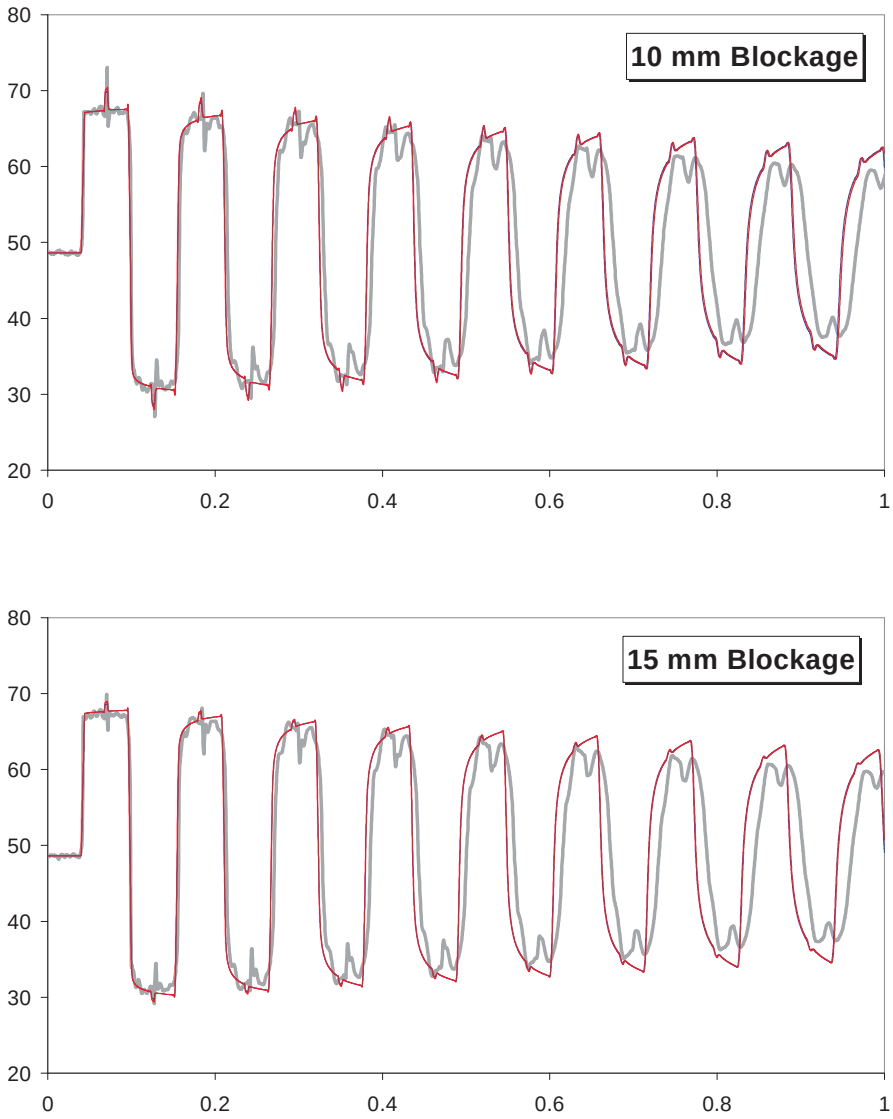

Figure 8.31 Comparison of Measured Data and Simulation Results for the Frequency-Dependent model at the WE under the Test Condition 5 (continued)

(The thick gray line: measured data, the blue line: steady blockage model, the red line: frequency-dependent model, x-axis: measurement time (s), and y-axis: pressure head (m))

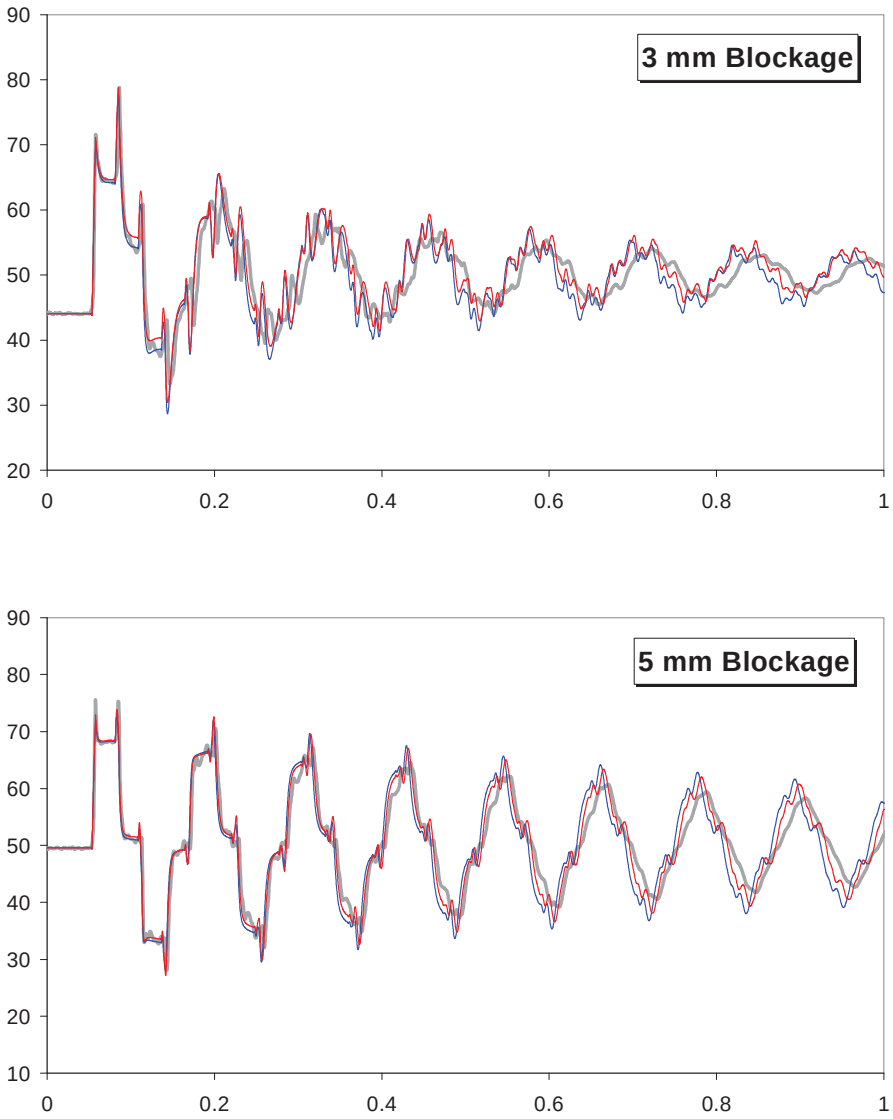

Figure 8.32 Comparison of Measured Data and Simulation Results for the Frequency-Dependent model at the WM under the Test Condition 5

(The thick gray line: measured data, the blue line: steady blockage model, the red line: frequency-dependent model, x-axis: measurement time (s), and y-axis: pressure head (m))

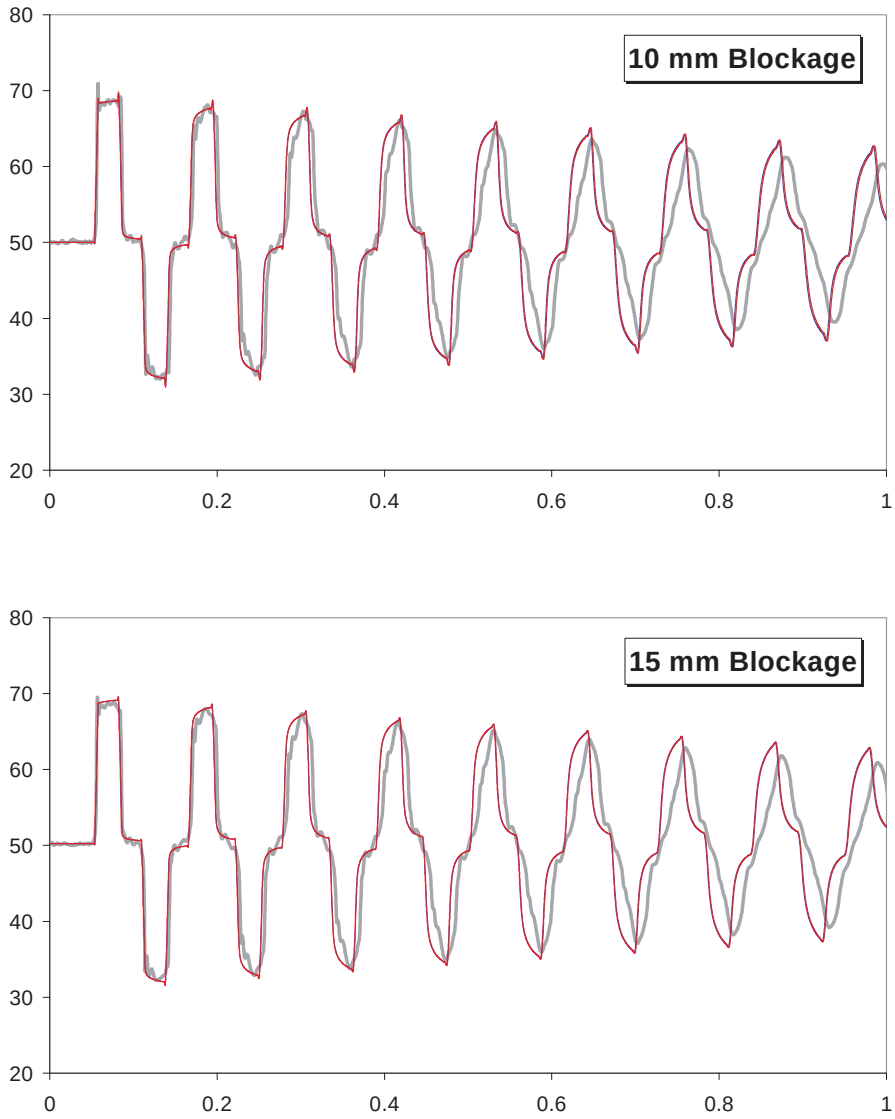

Figure 8.32 Comparison of Measured Data and Simulation Results for the Frequency-Dependent model at the WM under the Test Condition 5 (continued)

(The thick gray line: measured data, the blue line: steady blockage model, the red line: frequency-dependent model, x-axis: measurement time (s), and y-axis: pressure head (m))

8.5.1 Wavespeed Adjustment Method for Wavespeed Delay Phenomena

The pressure wave delay due to the slowing of the wave front as is passes through a restriction can be simulated by two different wavespeed adjustment methods based on the measured wavespeed. The first is to consider the inertia length of turbulent jet flow to define the zone of eddy inertia as shown in Fig. 8.33 when the pipeline has a flow restriction. Table 8.10 shows the measured wavespeeds according to the zones in the experimental pipeline shown in Fig. 8.8. Wavespeed #1 is measured between WM and

WE, wavespeed #2 is measured between WM and EM, and wavespeed #3 is measured between EM and EE by using the transmission time of the first pressure rise when transients are generated at WE. The local wavespeeds are an approximate measure because it is difficult to obtain an exact wavespeed between two measurement points (especially, in the eddy inertia zone because of the short length).

The values of wavespeed #1 are almost similar to the value of intact (or unblocked) pipeline shown in Table 8.7. The wavespeeds abruptly decrease in the eddy inertia zone and the values recover after the restrictions. These local wavespeeds of the zones can be used for unsteady minor loss flow analysis to adjust actual system wavespeeds. However, it is not easy to find exact local wavespeeds and their lengths theoretically or experimentally. The alternative method is to use the overall wavespeed of a pipeline system. The overall wavespeed can be easily obtained by measured data. Fig. 8.34 shows a comparison of measurement data for a 2 mm orifice flow and the simulation results by the wavespeed adjustment method using the overall wavespeed and the frequency-dependent model. The results in Fig. 8.34 show better agreement in the phase of pressure wave when compared to the 2 mm orifice result of Fig. 8.29 by using only the frequency-dependent model.

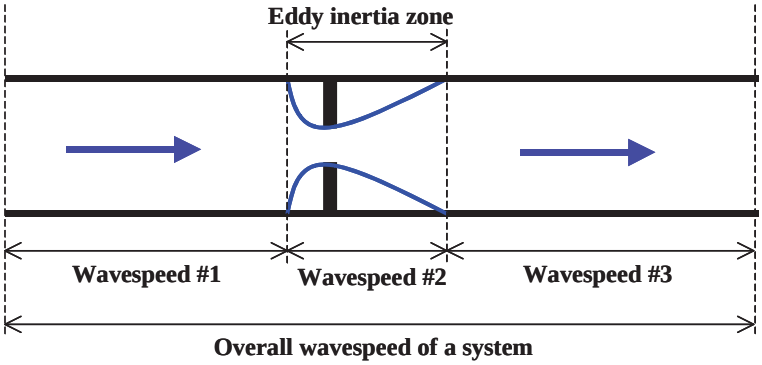

Figure 8.33 Zones of Different Wavespeeds

Table 8.10 Wavespeeds according to the Zone

	Overall Wavespeed (WE-EE) (m/s)	Wavespeed #1 (WE-WM) (m/s)	Wavespeed #2 (WM-EM) (m/s)	Wavespeed #3 (EM-EE) (m/s)
2 mm Orifice	1205.7	1329.8	620.8	1264.3
3 mm Orifice	1319.7	1324.3	1033.3	1220.7
3 mm Blockage	1203.3	1322.0	477.6	1264.3
5 mm Blockage	1296.9	1326.4	775.4	1297.5

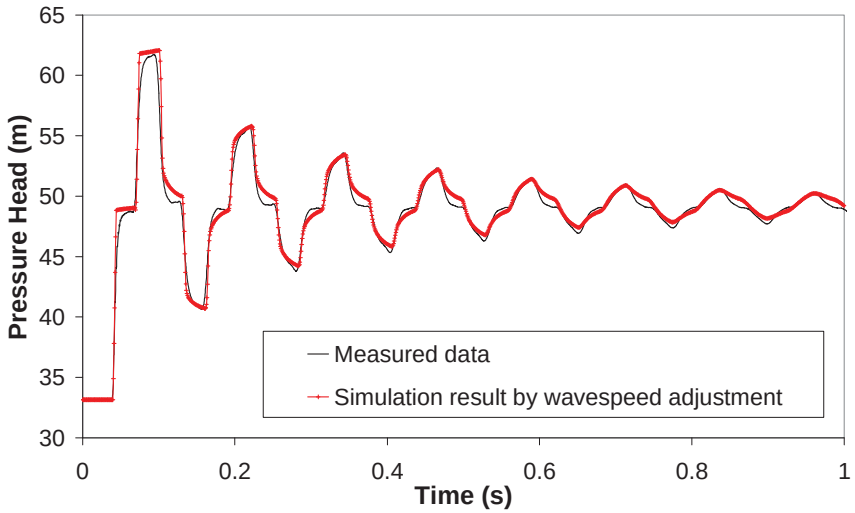

Figure 8.34 Simulation Result by Wavespeed Adjustment

8.6 SUMMARY AND CONCLUSIONS

In this study, the dynamic behaviour through an orifice or blockage (axial-extended orifice) has been represented by three different energy loss factors including the irreversible energy loss (net or permanent pressure loss) by turbulent jet flow, the kinetic pressure difference represented by the instantaneous flow acceleration and deceleration, and pressure wave dispersion by eddy inertia of the jet flow. The study proposes two different models to evaluate the unsteady kinetic pressure difference. One is the instantaneous inertia model based on a time dependent description of the dynamic response of a restriction. The other is a frequency-dependent model based on the rate of velocity changes at a restriction and the weighting function for the velocity changes. The traditional steady-state characteristics of an orifice have been used to calculate the net pressure loss. Finally, the wave dispersion by the eddy inertia of turbulent jet flow has been considered by the wavespeed adjustment method.

The transfer function for the kinetic pressure difference has been solved with the aid of the Laplace transform and the results of wave phenomena have been given in the frequency domain. The transfer function has no direct solution for the inverse Laplace transform to find the time domain properties (convolution weighting function for the velocity change at a restriction) for unsteady kinetic pressure difference. As a result, this research uses a numerical inversion of the Laplace transformation by approximating the transfer function. The overall procedure obeys the linear time-invariant system theory.

The measured data show that the magnitude of pressure wave dramatically decreases as the bore size of an orifice or blockage decreases. The most important characteristics are the apparent change in the wavespeed illustrated by the lagging and phase change of the pressure wave due to the reduction of bore size. Unlike the orifice behaviour, blockages generate high frequency pressure spikes because of the sudden change of pipe wall thickness. The simulation results for orifices and blockages by a steady model and the proposed unsteady kinetic pressure difference models without wavespeed adjustment method are almost same. The results of the frequency dependent model show slightly more pressure damping and dispersion of travelling pressure wave when compared to the results of steady state model. The results support the validity of the traditional view that the characteristic of an unsteady orifice flow can be approximately represented by a steady state model. However, the steady state model cannot calculate the wave delay effect. The simulation results of the frequency dependent model with wave adjustment show good agreement with the measured data in terms of the magnitude, shape and overall pressure trace.